Dalton Transactions

ROYAL SOCIETY OF CHEMISTRY

PERSPECTIVE

View Article Online
View Journal | View Issue

Cite this: *Dalton Trans.*, 2024, **53**, 17409

Optical detection strategies for Ni(II) ion using metal–organic chemosensors: from molecular design to environmental applications

Sudhanshu Naithani,[a] Ritesh Dubey, *[a] Tapas Goswami,*[a] Franck Thetiot*[b] and Sushil Kumar *[a]

Nickel is an important element utilized in various industrial/metallurgical processes, such as surgical and dental prostheses, Ni–Cd batteries, paint pigments, electroplating, ceramics, computer magnetic tapes, catalysis, and alloy manufacturing. However, its extensive use and associated waste production have led to increased nickel pollution in soils and water bodies, which adversely affects human health, animals and plants. This issue has prompted researchers to develop various optical probes, hereafter luminescent/colorimetric sensors, for the facile, sensitive and selective detection of nickel, particularly in biological and environmental contexts. In recent years, numerous functionalized chemosensors have been reported for imaging Ni^{2+}, both *in vivo* and *in vitro*. In this context, metal-based receptors offer clear advantages over conventional organic sensors (*viz.*, organic ligands, polymers, and membranes) in terms of cost, durability, stability, water solubility, recyclability, chemical flexibility and scope. This review highlights recent advancements in the design and fabrication of hybrid receptors (*i.e.*, metal complexes and MOFs) for the specific detection of Ni^{2+} ions in complex environmental and biological mixtures.

Received 21st August 2024,
Accepted 17th September 2024

DOI: 10.1039/d4dt02376e

rsc.li/dalton

1. Introduction

Group 10 metals such as nickel (Ni), palladium (Pd) and platinum (Pt) are widely used in various critical aspects of human life, including industries, material science, medicine and biology.[1–8] They are typically employed in the manufacturing of various electrical components, alloys and pharmaceuticals, among others.[1,9–15] Due to the distinct reactivity of the ionic forms of these metals, a significant range of related (bio)active molecules has been designed and developed.[16] However, mishandling and/or overuse of these metals has caused serious contamination in our ecological systems, particularly in soil and water systems, with significant environmental and biomedical consequences.[4,17–24]

Among the group 10 metals, nickel is essential for human life due to its involvement in various metabolic processes.[6,25,26] However, both nickel deficiency and excess intake are associated with numerous health effects. For instance, a concentration exceeding 0.07 mg L^{-1} of nickel in the body can lead to lung fibrosis, dermatitis, asthma, cancer, and other allergic reactions.[17,27] Furthermore, nickel compounds have been classified as 'category 1 carcinogens' to humans by the International Agency for Research on Cancer (IARC) since 1990.[28] Consequently, the World Health Organisation (WHO) has established a concentration limit of 0.02 mg L^{-1} for Ni-based ions in drinking water.[29] Hence, there is an urgent demand to develop rapid, effective, and reliable methods for detecting Ni(II) ions, particularly in environmental and biological samples.

In contrast to conventional techniques,[30–35] optical (luminescent or colorimetric) detection methods have gained considerable attention from researchers due to their advantages of rapid (less than 10 min or instantaneous), sensitive (*i.e.*, ppb level), non-destructive facile recognition of various metal ions and other biologically or environmentally important analytes.[18,36,37] Conceptually, an optical sensor consists of three key components: (i) a binding unit or receptor to display specific binding with the target analyte; (ii) a photoactive unit to emit a signal in the form of luminescence or chromogenic response upon analyte–receptor interaction and (iii) a spacer group or linker to regulate the electron/energy transfer between the receptor and the photoactive unit.[38] Optical sensors may be commonly classified into two categories depending on the signal emitted from their photoactive unit or signaling unit, as follows: (i) luminescent sensors, with the

[a]*Department of Chemistry, School of Advanced Engineering (Applied Science Cluster), UPES, Dehradun-248007, Uttarakhand, India.*
E-mail: sushil.k@ddn.upes.ac.in, tgoswami@ddn.upes.ac.in
[b]*CEMCA, CNRS, UMR 6521, Université de Bretagne Occidentale, Brest 29238, France*

ability to display distinct luminescence responses in the presence or absence of an analyte,[39] which is significant for dynamic monitoring, and (ii) the colorimetric sensors, which allow the naked-eye detection of guest analytes based on color changes. To some extent, colorimetric sensors may be comparatively deemed more promising due to their simplicity, on-site and real-time analysis, and relatively lower capital cost.[40]

Thus, over the past few years, a broad range of luminescent and colorimetric probes based on small organic[41–45] and inorganic molecules,[46–48] metal–organic frameworks (MOFs)[49–51] and nanomaterials[52–55] has been specifically developed for the recognition of Ni(II) ions. Distinctive from the typical organic sensors, metal-based probes tend to exhibit improved cation sensing and selectivity properties. Additionally, metal-based receptors and their implicit highly flexible chemistry and design (structure, nature, *etc.*) show some compelling features including notably rich and fine tuning of their optical properties (*e.g.*, absorption/emission in the visible region), redox- and photostability, magnetism, catalysis, and improved solubility in aqueous medium.[56–60] Also, the integration of these features into sensor technology is indirectly paving the way for multifunctional platforms with diverse viable applications. Therefore, this work aims to summarize the state-of-the-art in the development of both luminescent and colorimetric probes, specifically metal–organic probes for the detection of Ni^{2+} ions, highlighting their recent developmental progress. Contextually, to the best of our knowledge, the optical detection of Ni^{2+} by various types of metal-based receptors (*e.g.*, metal complexes and MOFs) has not been extensively reviewed to date. Indeed, several reviews have been recently reported on the fluorometric and colorimetric detection of Ni^{2+} ions;[61–63] however, they were dedicated to organic fluorophores or restricted to one specific type of probe such as ratiometric and near-infrared (NIR) based probes. Hence, an updated inventory of the receptors reported in the last 25 years for the specific detection of Ni^{2+} has been assessed and systematically ordered by the incremental intricacies of the probes ranging from metal complexes to MOFs. Finally, the existing probe design opportunities, challenges and promising development prospects are presented.

2. Probe design: luminescent *vs.* colorimetric probes

Integrating an organic or inorganic (*e.g.*, metal complex)-based chromophore with a specific receptor is the prototypical approach to design a cation-responsive luminescent or colorimetric probe. In these probes, the binding of metal ions to the receptor consistently alters its luminescence, absorbance and/or relaxivity,[38,64] confirming the presence of the guest analyte (*i.e.*, metal ion). For these receptors to be functional, either intermolecular or intramolecular interactions between the signaling unit and the receptor unit are required, with an implicit distinction between luminescent and colorimetric probes.[40,64] Indeed, luminescent sensors are typically related to various photoinduced electron/energy transfer processes. Several mechanisms, notably PeT (photoinduced electron transfer),[65–67] PCT (photoinduced charge transfer)[68,69] and FRET (fluorescence resonance energy transfer),[70,71] have been explored and frequently adopted to design luminescent molecular probes. Alternatively, several other mechanisms, *e.g.*, metal-bound inhibited ESIPT (excited-state intramolecular proton transfer)[72,73] and AIE (aggregation-induced emission),[74–76] have also been established for the design of these probes. Among these mechanisms, PeT is considered the typical mechanism for most of the reported cation-responsive luminescent probes, while the intramolecular charge transfer (*i.e.*, ICT) process is commonly observed for colorimetric probes, and thus the only PeT and ICT mechanisms are further detailed hereafter.

2.1 PeT process in luminescent probes

A typical PeT probe consists of three important components, *i.e.*, a signaling unit (*i.e.*, luminophore), a spacer unit (*i.e.*, linker) and a receptor (*i.e.*, ionophore or binding unit) (Fig. 1).[38,77] Usually, the ionophore is an electron (e^-) donor such as thio- or amino- containing groups, whereas the luminophore acts as an e^- acceptor. In the case of the free probe (without guest analyte) (Fig. 1(a)), an e^- present in the HOMO (highest-occupied-molecular-orbital) of its luminophore is promoted to the LUMO (lowest-unoccupied-molecular-orbital) with the absorption of a photon of suitable wavelength (excited luminophore). If the energy level of the HOMO of the free ionophore is slightly higher than the HOMO of the luminophore, spatial electron transfer will take place from the ionophore to the luminophore through HOMOs (Fig. 1(a)). Consequently, the transition of the excited electron from the LUMO to HOMO of the luminophore is blocked; this quenching of emission is defined as the PeT process.[78,79] Metal ion binding to the ionophore results in a decrease in the HOMO energy of the ionophore below the HOMO level of the luminophore, ultimately restoring the luminescence response of the probe (Fig. 1(b)). This phenomenon of luminescence recovery

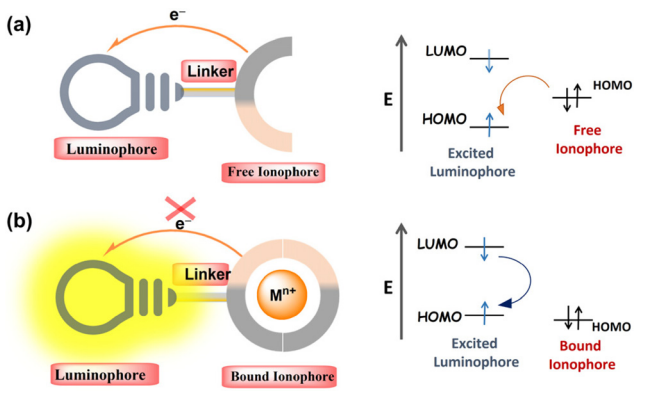

Fig. 1 Schematic "turn-on" sensing mechanism in PeT luminescent probes for metal ion targets; (a) free probe and (b) probe with target metal ion.

is also known as the metal-chelation-enhanced-luminescence effect.[77–79] The restoration of the luminescence and the emission of the resultant metal complex is often attributed to the π → π* excited-state relaxation of the luminescence. Notably, the protonation of the ionophore group may also block the PeT event.[80]

Over the past 30 years, numerous cation-responsive luminescent PeT probes have been documented in the literature. However, PeT-based probes may still display shortcomings, and thus there are still developmental obstacles that need to be addressed. For instance, although near-infrared (NIR)-active probes are gaining increasing attention from researchers due to their deep tissue-penetration ability and relatively low phototoxicity, they suffer from low analyte-induced-emission-enhancement factor and large background luminescence.[81,82] Indeed, in the case of NIR probes, generally a higher HOMO energy level of the luminophore reduces the energy gap between the HOMOs of the luminophore and ionophore. As a result, the PeT process becomes less efficient to quench the emission of the free probe. Hence, the development of 'turn-on'-responsive NIR probes with the PeT mechanism and low background is still a challenging but pertinent task.[83] Moreover, the alternative two-photon (TP) excitable PeT probes may be emphasized to achieve practical bio-imaging applications.[84]

2.2 ICT process in colorimetric probes

Distinct from luminescent receptors, colorimetric sensors are associated with changes observed in their electronic properties in the form of inter- or intramolecular charge transfer (ICT), *e.g.*, ligand-to-metal-charge-transfer (LMCT) and metal-to-ligand-charge-transfer (MLCT) transitions (Fig. 2).[85] A molecular sensor with the D–π–A system is commonly used to accomplish the colorimetric sensing of metal ions. Further, the D–π–A molecular system can be obtained by introducing both electron donor (D) and electron acceptor (A) groups in the molecular sensor at suitable positions. Metal ion binding to either D or A in the molecular probe occurs *via* the hard and soft acid and base (HSAB) principle.[86] In general, the metal ion binding to D reduces its electron-donating ability, ultimately converting the D–π–A molecular system to A–π–A; as a result, the conjugation of the system is reduced, leading to a blue-shift in the absorption spectrum of the probe (due to the occurrence of an LMCT transition) (Fig. 2(a)).[85,87] Comparatively, metal ion binding to the A moiety endows the D–π–A system with remarkable strength, leading to an increase in the push–pull intramolecular charge transfer effect with a concomitant red-shift in its UV-Vis spectrum (due to the occurrence of an MLCT transition) (Fig. 2(b)).[85,88] These types of cation-induced transitions together with ICT contribute to the color changes observed after binding with the target.

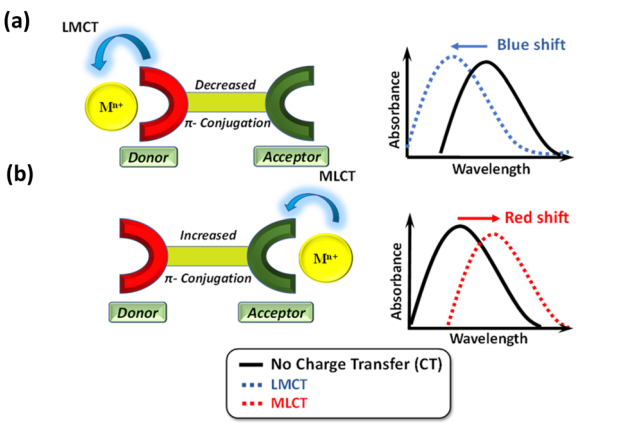

Fig. 2 Distinct binding effects of metal ions on D–π–A system of colorimetric probes with a concomitant shift in UV-Vis spectra due to (a) LMCT and (b) MLCT transitions.

A systematic evaluation of various sensors prompted us to discern the optical behaviors of different metal-based sensors towards the target analytes. It was noticed that in most cases, metal complexes and MOFs rely on the PeT mechanism for the luminescent detection of metal ions. This review mainly focuses on the recent progress and limitations to date in the development of Ni^{2+}-responsive probes. Thereafter, the luminescent and colorimetric metal-based receptors for Ni^{2+} ions are assessed and described with their photophysical behaviors. The selected probes are carefully classified based on their progressive intricacies as the first criterion, ranging from metal complexes to MOFs. Besides, perspectives are presented in an attempt to further rationalize the development and optimization processes of these luminescent and colorimetric metal-based receptors.

2.3 Fundamental aspects for Ni^{2+} selectivity

The design of the binding motif (or receptor) in a cation-responsive probe is a crucial parameter to achieve selectivity for a specific metal ion (*i.e.*, target analyte) over other competing species. To improve the receptor-cation interaction and the metal ion selectivity, the following aspects must be notably considered:

(i) *Size of the receptor pocket*: the effective ionic radius of the Ni^{2+} ion may vary between 49.0 pm and 69.0 pm depending on the number and nature of the coordinating ligands.[89] Hence, a selective probe for Ni^{2+} ions can be achieved by fine tuning the receptor pocket within this range; concurrently, it should exclude the risk of the probe response/affinity towards larger or shorter cations or other competing species.

(ii) *The nature and number of donor atoms in the receptor unit and (iii) the geometry of the receptor pocket*: Ni^{2+} is a first-row transition metal ion with a d^8 electronic configuration. It has a tendency to form tetrahedral, square planar, and octahedral complexes. Notably, the square planar geometry is dominant over the tetrahedral geometry, and thus a receptor pocket bearing strong-field ligands and four donor sites must be incorporated in the Ni^{2+} core. Therefore, Ni^{2+}-responsive probe must typically include aliphatic amines, carbonyls, pyridine, 2,2′-bipyridine or 1,10-phenanthroline in its receptor unit.[61] On the contrary, the ligand field strength has less impact on Ni^{2+} octahedral complexes due to the identical

filling of electrons in either low-spin or high-spin d^8 complexes.

(iv) *The hard and soft basicity of donor atoms in the receptor*: the magnitude of the cation–receptor interaction directly depends on both the cation and donor atoms in the receptor. The hard and soft acid and base (HSAB) principle may be implemented to design ideal probes with strong cation–receptor interactions. Ni^{2+} is a borderline (neither hard nor soft) acid, paramagnetic and quite similar in size with neighbouring elements in the periodic table. Therefore, the design of highly selective probes for Ni^{2+} is still a challenging task. Because of its borderline acid character, Ni^{2+} prefers to interact with borderline bases such as imidazole and pyridine donors, tertiary amines, azides, and sulfites. Hence, these groups should be incorporated into the receptor units of Ni^{2+}-responsive probes. Furthermore, to achieve high cation selectivity, the function of solvent and pH of the medium as well as its composition (*e.g.*, presence of competing or interfering species in the medium) should not be ignored. Indeed, a slight change in pH or solvent can remarkably tune or alter the sensing ability of the resultant probe for a particular metal ion.

Finally, to design a metal ion-responsive probe, the ideal situation is to identify a robust binding unit or receptor for the target cation. These receptors typically display the same selectivity to the metal, regardless of the luminophores to which they are tethered. This strategy has been successfully achieved and implemented for some transition metal ions *e.g.*, Cu^{+} and Zn^{2+} ions.[67,90,91] Most of the Cu^{+}-responsive probes contain thioether-rich receptors,[92] while Zn^{2+} could be selectively detected by probes having dipicolylamine (DPA)-based binding motifs.[93,94] The recognition by these robust receptors enables the development of a library of cation-responsive probes with finely tuned physicochemical and biological properties.

3. Ni^{2+} ion: general features and impact

The industrial demand for nickel (Ni) has dramatically expanded over the last century, resulting in increased pollution and health concerns. Ni^{2+} is utilized in a wide range of metallurgical, environmental, medicines and catalytic processes (*e.g.*, fuel cells, alloys, Ni–Cd batteries, ceramics, dental prostheses, and catalysts).[52,95,96] However, excess Ni^{2+} in the body can cause allergic contact dermatitis, asthma, conjunctivitis, pneumonitis, lung fibrosis, *etc*. Also, long-term Ni^{2+} exposure (*via* inhalation, dietary intake, water sources, *etc*.) has been linked to cancers of the lungs, nose, sinuses, stomach, and throat.[17,61,97,98] Although the impact of the Ni^{2+} concentration in living beings is still not fully understood, it is known that excessive Ni^{2+} exposure may generate harmful health consequences. Alternatively, Ni^{2+} is an essential co-factor for many enzymes that play crucial roles in microorganisms (such as bacteria, fungi and algae) and plants.[99,100] It also participates in various cellular processes, especially energy-related processes and nitrogen metabolism. In comparison to other biorelevant metal ions, the use of Ni^{2+} is found limited but consistent in eukaryotes.[101] To date, only a few Ni-containing enzymes such as [NiFe]hydrogenase, urease and Ni-SoD (Ni-superoxide dismutase), have been explored.[102,103] In contrast, these enzymes are mainly involved in cellular processes of microbes, but no Ni-containing enzyme has been discovered in mammals thus far.[99,100] Consequently, the detection of Ni^{2+} in the environment and biological systems is critical. Small molecule-based optical sensors can detect and quantify metal ions in a wide range of samples, ranging from cell organelles to all water bodies. Beyond detection, it is also significant and necessary to understand both the physiological and psychological aspects and impacts of Ni^{2+} ions.

4. Metal complex-based sensors

Metal complexes have been extensively investigated for optical sensing of metal ions given that they possess a large Stokes shift, excellent redox and photophysical properties, remarkable photostability and absorption/emission in the visible region.[56–60] In general, these sensors consist of a ligand system with a single metallic core as the luminophore. To date, most studies on metal complexes as cation-responsive probes have been essentially related to specific transition metals, namely Mn^{2+}, Zn^{2+}, Co^{3+}, Cu^{2+}, and Ru^{2+} complexes.[104–107] More recently, complexes involving lanthanides (Ln^{3+}) have also emerged as an intriguing alternative in the sensing field.[108–112] In many cases, the emphasis has been the mechanistic pathway of cation sensing involved in these probes. In these complexes, the receptor is usually linked to the metal core either *via* a σ or π linker. Thus, cation binding to the receptor alters the optical characteristics (luminescence or absorbance) of the corresponding metal complex.[113] In luminescence sensing, this interaction usually allows the metal complex to serve as either a 'turn-on'- or 'turn-off'-type sensor. The binding unit having conjugation with the metal core *via* a π linker may also lead to a change in the emission wavelength of the metal complex upon target binding. Alternatively, the colorimetric sensors display a color change upon the addition of the analyte.[114]

4.1 Luminescent Ni^{2+} sensors

The development of new luminescent sensors for the quick and easy detection of Ni^{2+} is appealing. To the best of the our knowledge, the first report on a metal-based receptor for the luminescence sensing of Ni^{2+} ions was presented by Bolletta *et al.* in 1999.[115] In their study, a Ru^{2+}(bpy) complex (**1**) based on a dioxo-tetramine ligand (*i.e.*, tetra-aza macrocycle) acted as a luminescent probe for Cu^{2+} and Ni^{2+} ions in aqueous medium (Fig. 3). The sensing ability of probe **1** was assessed by monitoring the alterations in its luminescence intensity and excited-state lifetime as a function of pH, with and without Ni^{2+} ions. In the absence of Ni^{2+}, the luminescence intensity of probe **1** remained constant in the pH range of

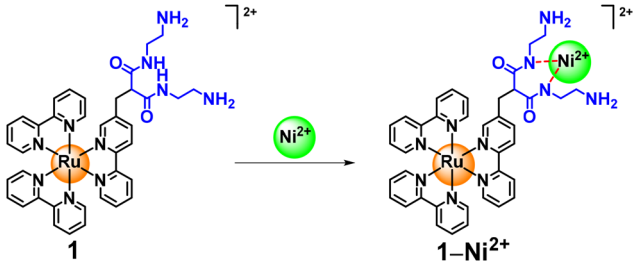

Fig. 3 Binding mode of Ru^{2+}-based probe **1** towards Ni^{2+} in aqueous phase.

2.0–12.0. In this pH range, the emission quantum yield (Φ_{em} = 0.030) and the excited-state lifetime (t = 440 ns) of **1** were similar to that found for the prototype complex, *i.e.*, $[Ru(bpy)_3]^{2+}$, in aqueous medium. These results clearly indicated that the dioxo-tetramine ligand showed no remarkable perturbance to the excited-state characteristics of the Ru^{2+}-bpy fragment. On the contrary, upon the addition of Ni^{2+} ions to **1** in a 1 : 1 molar ratio, a typical sigmoidal profile was observed in the plot of luminescence intensity *vs.* pH of the medium. The decrease in the excited-state lifetime to 11.0 ns clearly indicated the strong intramolecular luminescence quenching of probe **1** in the presence of Ni^{2+} ions. The authors anticipated that the luminescent intensity was quenched due to the energy transfer process with a steady-state quenching constant of 2.1 × 10^7 s^{-1}.

Later, in 2009, Mukherjee's group[116] developed luminescent molecular rectangle **2** for potential applications toward cation recognition (Fig. 4). The four N atoms from the imine (–CH=N–) groups in the core enable probe **2** to act as a suitable receptor for moderately hard transition metal ions such as Ni^{2+}, Cu^{2+}, and Mn^{2+}. The 1,8-platinum-functionalized anthracene units were referred to as 'molecular clips', and the presence of the ethynyl functionality in the structure of the probe induced the luminescence behavior of the luminophore

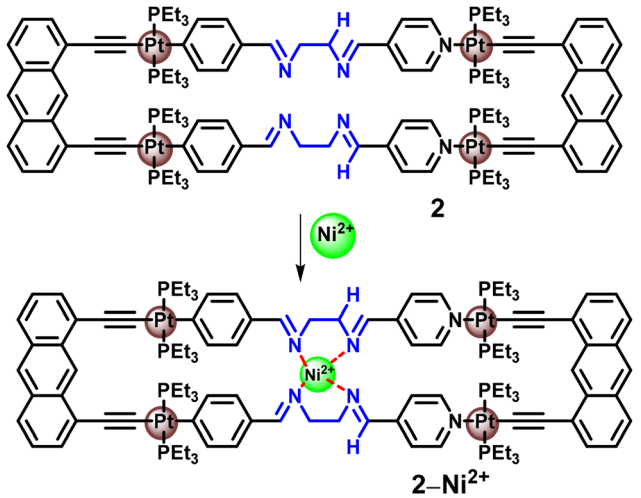

Fig. 4 Binding mode of Pt-based probe **2** towards Ni^{2+} in methanol.

in this probe. The UV-Vis spectrum of **2** in methanol displayed an intense absorption peak at 258 nm, which was ascribed to the intraligand π → π* transition. In addition, low-intensity absorptions were also observed at 424 nm, 400 nm, 380 nm and 353 nm. Upon excitation with 400 nm light, probe **2** emitted at approximately 460 nm in methanol (*ca.* 3.0 × 10^{-5} M). The luminescence intensity of **2** was significantly quenched upon titration with Cu^{2+} and Ni^{2+}, exhibiting PeT as the possible mechanistic pathway for the quenching event. Interestingly, the luminescence of **2** could easily be revived with the addition of 2,2′-bipyridine to a solution of the **2**-Ni^{2+} adduct.

In the subsequent year, probe **3** was reported by Li *et al.*,[46] which was the first metal-based probe exclusively selective for Ni^{2+} ions (Fig. 5). This probe was comprised of a Zn^{2+}-based coordination compound with a multifunctional symmetrical Schiff base as the ligand scaffold. The emission of this probe could be seen at 363 nm when excited at 295 nm in 10^{-5} M DMF (*N*,*N*′-dimethylformamide) solution. The addition of 1.0–3.0 equiv. of Ni^{2+} resulted in an enhancement in the luminescence of probe **3**, whereas its luminescence decreased in the presence of other metal ions, *e.g.*, Cu^{2+}, Mn^{2+}, Al^{3+}, K^+, Mg^{2+}, Cd^{2+} and Na^+ ions. The binding of Ni^{2+} to **3** was further supported by the single-crystal X-ray diffraction (SC-XRD) study, leading to the description of **3**-Ni^{2+} as a heterometallic trinuclear compound. The authors anticipated that the incorporation of two Ni^{2+} ions provided additional rigidity to the probe, which reduced the energy loss occurring due to vibrational motions.

In the same year (2012), the Tian, Sun and group[48] constructed a ligand in which a terpyridine (tpy) unit was linked with a triazole unit through a phenyl linker (Fig. 6). It is well known that the tpy moiety displays relatively stronger binding with borderline acids such as Zn^{2+} compared to the triazole unit. Consequently, the treatment of this ligand with a Zn^{2+} salt afforded the formation of complex **4** having two tpy units coordinated to the metal centre. The crystal structure analysis of **4** clearly revealed that the tpy rings slightly deviated from the plane of the phenyl linker, ultimately resulting in intense luminescence and efficient energy transfer process. The luminescence sensing ability of **4** towards different metal ions was carried out in DMF solution. Other metal ions such as

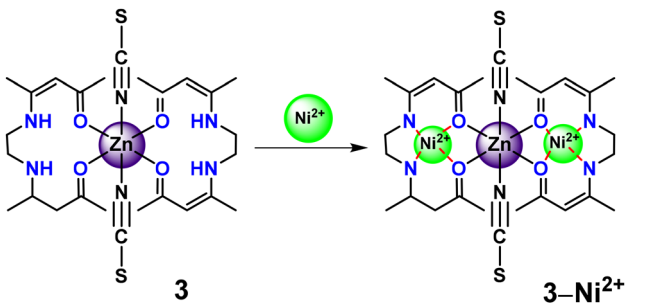

Fig. 5 Binding mode of Zn-based supramolecular probe **3** with Ni^{2+} in DMF solution.

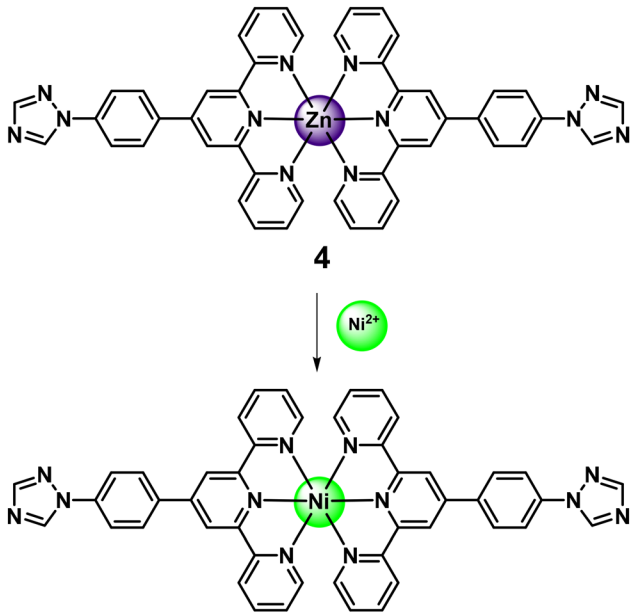

Fig. 6 Detection of Ni^{2+} ions by the displacement of the central atom in Zn-based probe **4**.

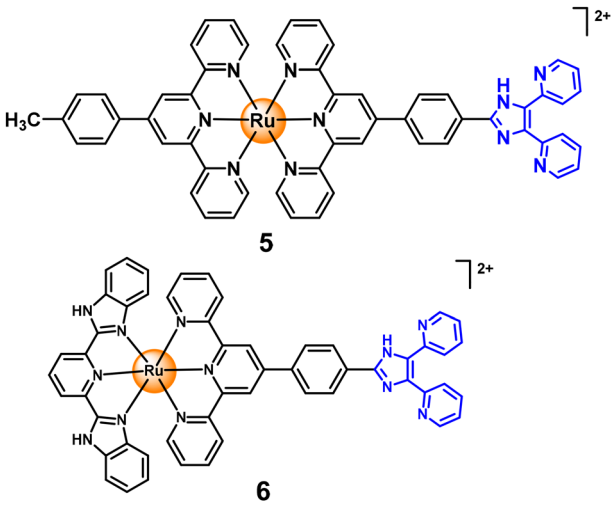

Fig. 7 Chemical drawings of probes **5** and **6**.

$Fe^{2+/3+}$, Cu^{2+}, Zn^{2+}, Cd^{2+} and In^{3+} induced a small emission quenching at 360 nm (λ_{ex} = 291 nm), which could be attributed to either the paramagnetic nature of the related metals or electron/energy transfer processes. On the contrary, Co^{2+} and Ni^{2+} ions triggered the complete luminescence quenching of probe **4**. ESI-MS measurements were performed to gain better insight into the luminescence quenching caused by the addition of Ni^{2+} ions. The molecular ion peak of $[Zn(L)_2]^{2+}$ at *m*/*z* 408.28 disappeared in the ESI mass spectrum of **4**-Ni^{2+}; however, a new peak at *m*/*z* 405.33 corresponding to $[Ni(L)_2]^{2+}$ appeared. It was suggested that Ni^{2+} and Co^{2+} ions could replace Zn^{2+} in **4** and bind strongly with the tpy unit, leading to complete luminescence quenching, whereas weak coordination of the triazole unit could be realized in the case of other metals. Furthermore, the luminescence of probe **4** could not be revived upon the addition of EDTA (ethylenediaminetetraacetic acid), indicating the strong affinity of the tpy moiety for the Ni^{2+} ion.

In 2018, Baitalik's group[117] developed two bis-tridentate Ru (II) probes **5** and **6** based on tpy derivatives as ligands to investigate their cation-responsive behaviors (Fig. 7). The main ligand frame consisted of a tpy moiety linked with a pyridine-imidazole group *via* a phenyl linker. The absorption and emission spectra of **5** and **6** were recorded in different organic solvents such as dichloromethane (DCM), methanol, ethanol, acetonitrile (ACN or CH_3CN) and dimethylsulfoxide (DMSO), and the comprehensive spectral features of these probes were discussed in detail. The UV-Vis spectra of **5** and **6** displayed sharp bands in the range 230–293 nm due to the ligand centred $\pi \rightarrow \pi^*$, transition while a metal-to-ligand-charge-transfer (MLCT) band was observed between 491 nm and 508 nm. In addition, one intraligand charge transfer (ILCT) band was noticed between 311 nm and 354 nm in the UV-Vis spectra of both **5** and **6**. The emission maximum was observed at 660 nm for **5** and 688 nm for **6** when excited at 490 nm in DMSO solution. Both probes exhibited emission at room temperature and at low temperature (77 K), having excited-state lifetimes in the range of 0.5 to 70.0 ns (nanoseconds), eventually relying on the solvent as well as the co-ligands. The spectral changes in the absorption and emission spectra of the probes were monitored in the presence of various metal ions such as Mn^{2+}, Fe^{2+}, Co^{2+}, Ni^{2+}, Cu^{2+}, Zn^{2+}, Pb^{2+}, Cd^{2+} and Hg^{2+} in CH_3CN solution. The MLCT band remained intact in both probes upon the addition of Mn^{2+}, Pb^{2+}, Co^{2+}, Cd^{2+} and Hg^{2+}, whereas a small decrease in its intensity was observed for Ni^{2+}, Fe^{2+} and Cu^{2+} ions. Notably, the absorption intensity of the ILCT band increased, in general, with the level of increase varying depending on the cations studied. Among the various metal ions, a very small luminescence enhancement was observed with Zn^{2+} for both probes, most probably due to the PeT process. The emission behavior of **5** and **6** remained roughly unaltered with Pb^{2+}, Hg^{2+} and Cd^{2+} ions, whereas remarkable quenching appeared in presence of Fe^{2+}, Ni^{2+} and Cu^{2+} ions.

Later, in 2021, Cui's group[118,119] developed two Co(II)-based luminescent probes, $[Co_2(L_1)(NPTA)]\cdot H_2O$ (**7**) and $[Co(L_2)(npth)]\cdot nH_2O$ (**8**) (where L_1 and NPTA represent 1,2-bis(thiabendazole-1-ylmethyl)benzene and 2-nitroterephthalic acid; L_2 and npth represent 1,1′-(1,6-hexanediyl)bis[2-(2-pyridyl)benzimidazole] and 3-nitroterephthalic acid, respectively), as Ni^{2+} receptors. The crystal structures of both **7** and **8** were depicted by SC-XRD study (Fig. 8). The luminescence behaviors of these probes towards various cations and anions were investigated in the solid-state and solution phase at room temperature. The emission maximum for **7** and **8** was centred at 378 nm (λ_{ex} = 298 nm) and 381 nm (λ_{ex} = 299 nm), respectively, in the solid-state at room temperature. The dispersion of probe **8** in water did not display any change in its luminescence intensity even after 100 min, which suggested the stable nature of this probe in aqueous media. The luminescence intensity of probe **8** was

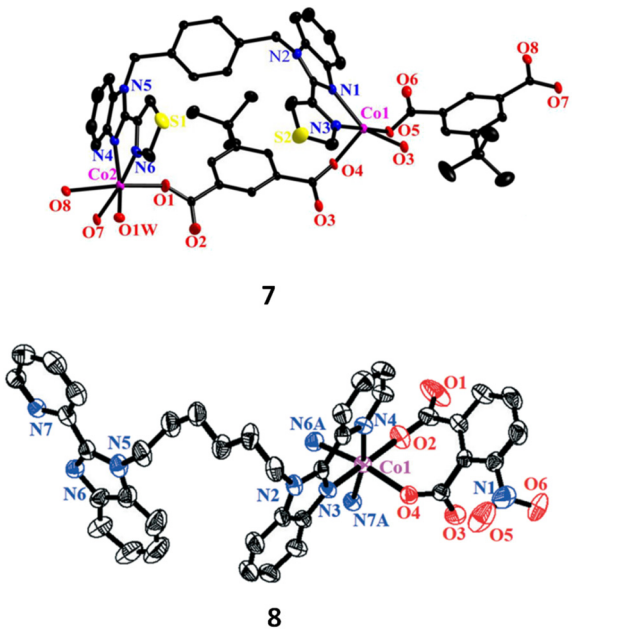

Fig. 8 Crystal structures of probes **7** and **8**. Adapted with permission from ref. 118. Copyright 2021, The Royal Society of Chemistry, and ref. 119, Copyright 2021, Springer.

highly influenced by diverse cations; however, substantial quenching (*ca.* 93%) was noticed solely for the Ni^{2+} ion. The selectivity studies exhibited that the quenching effect for Ni^{2+} was not interfered by other metal ions (such as K^+, Ag^+, Mg^{2+}, Al^{3+}, Ca^{2+}, Co^{2+}, Zn^{2+}, Sr^{2+}, Cd^{2+}, Hg^{2+}, Cr^{3+}, Fe^{3+}, Sm^{3+}, Eu^{3+}, Gd^{3+}, Tb^{3+} and Er^{3+}), and thus **8** displayed excellent selectivity for Ni^{2+} ions with an LoD value of 4.54 μM. Probes **7** and **8** were also explored for their sensing ability towards anionic species. Interestingly, **7** showed a selective luminescence response towards MnO_4^- over several competing anions (*e.g.*, Cl^-, Br^-, I^-, ClO_3^-, BrO_3^-, IO_3^-, NO_3^-, OCN^-, MnO_4^-, SCN^-, CO_3^{2-}, SO_4^{2-}, $H_2PO_4^{2-}$, HPO_4^{2-}, $Cr_2O_7^{2-}$ and $P_2O_7^{4-}$) with a remarkable quenching efficiency of *ca.* 97%. The emission decay lifetimes of **7** and **8** were depicted to be 1.737 μs and 3.837 μs, respectively, as evidenced by the bi-exponential fitting of the luminescence decay data. The luminescence quenching in **7** or **8** was attributed to either a photoinduced e^- transfer from the probe to Ni^{2+} (host to guest) or the competitive absorption of excitation light between **7**/**8** and the target Ni^{2+} ion.

Later, in the same year (2021), Han and group[120] reported a water-soluble zinc(II)-based coordination compound **9** that could detect Fe^{3+}, Cu^{2+}, Ni^{2+} and CrO_4^{2-} ions among diverse panels of cations and anions (Fig. 9(a)). Probe **9** exhibited its emission maximum centred at 371 nm upon excitation at 335 nm in water. Among the various cations studied, Fe^{3+} induced the maximum luminescence quenching in **9** at 371 nm, which was ascribed to the energy transfer and competitive wide absorption spectrum (200–400 nm) of the source, whereas the quenching mechanism of Ni^{2+} and Cu^{2+} ions was ascribed to the overlap of the excitation spectrum of the probe and the absorption of the cations studied (Fig. 9(b)). The

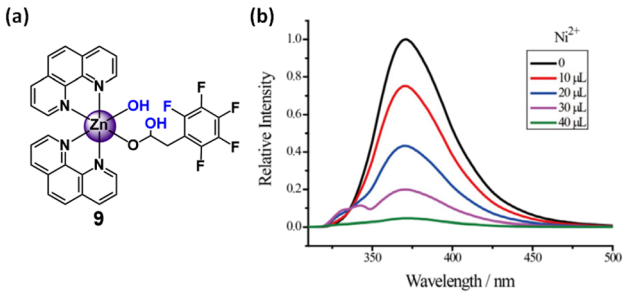

Fig. 9 (a) Chemical drawing of probe **9** and (b) luminescent quenching of **9** upon addition of Ni^{2+} ions in water. Adapted with permission from ref. 120. Copyright 2021, Elsevier.

Stern–Volmer constant (K_{sv}) value for Ni^{2+} was 2.68×10^4 M^{-1} with the LoD of 0.491 μM.

4.2 Colorimetric Ni^{2+} sensors

In an elegant study in 2004, Stang and co-workers[121] constructed supramolecular rectangular probe **10** for the rapid optical-based detection of Ni^{2+}, Cd^{2+} and Cr^{3+} ions in methanolic solution (Fig. 10). UV-Vis spectroscopy was employed to test the cation sensing ability of this probe. The absorption spectrum of **10** in methanol exhibited three major bands centred at 230 nm, 280 nm and 350 nm. Upon the addition of Ni^{2+} to the probe solution, remarkable changes were observed in the absorption spectrum of **10**, with one isosbestic point noticed at 300 nm. A 1 : 1 binding stoichiometry for the formation of complex **10**-Ni^{2+} was evidenced by the Job's plot and ESI mass analyses, and the binding constant was determined to be $2.01 \pm 0.05 \times 10^7$ M^{-1}.

In 2012, Molina, Tárraga and co-workers[47] reported a series of unsymmetrical di-substituted ferrocenes (**11**–**13**) containing triazole units developed using the Staudinger–aza Wittig

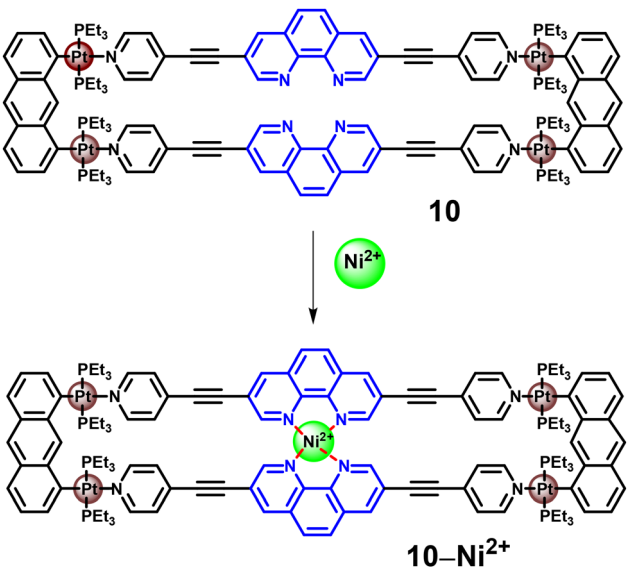

Fig. 10 Binding mode of Pt-based probe **10** towards Ni^{2+} in methanol.

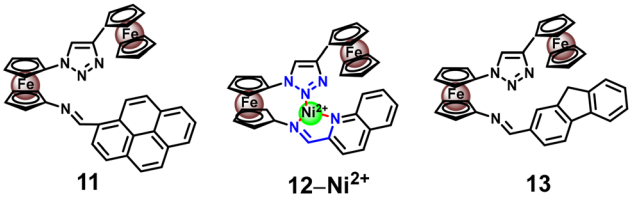

Fig. 11 Chemical structures of probes **11**-**13**, and binding mode of **12** with Ni^{2+} ions.

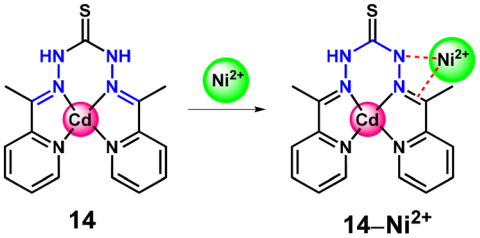

Fig. 12 Binding mode of Ni^{2+} with Cd(II)-based probe **14**.

process (Fig. 11). These complexes were explored as optical probes to detect various metal ions. Among the reported probes, **12** acted as a colorimetric sensor for Ni^{2+} and Cd^{2+} ions. The crystal structure of **12** was elucidated by SC-XRD analyses, exhibiting a monoclinic space group *Cc*, which was further corroborated with the help of DFT studies. UV-Vis spectroscopy displayed a high energy absorption band centred at 284 nm for **11**, 317 nm for **12**, and 336 nm for **13** in a mixture of organic solvents (CH_3CN/CH_2Cl_2). Two low energy bands responsible for the red color of the probes could also be seen in the range of 317–380 nm and 479–495 nm. These probes showed a half-wave potential value of $\Delta E_{1/2}$ = 0.02 V, $\Delta E_{1/2}$ = 0.26 V, and $\Delta E_{1/2}$ = 0.21 V for **11**, **12**, and **13** (Fc^+/Fc redox couple), respectively, with two reversible redox waves of one-electron. The redox potential of **11** and **13** was affected only by the addition of Pb^{2+} and Zn^{2+} ions among the investigated cations (*i.e.*, Li^+, Na^+, K^+, Ca^{2+}, Mg^{2+}, Ni^{2+}, Zn^{2+}, Pb^{2+}, Hg^{2+}, and Cu^{2+}). However, metal ions such as Ni^{2+}, Cd^{2+}, Zn^{2+}, and Pb^{2+} remarkably altered the redox potential of **12**. The response of these cations towards **12** was further investigated by UV-Vis studies in CH_3CN/CH_2Cl_2 solution, where significant changes were observed after the addition of Ni^{2+}, Cd^{2+}, Zn^{2+} and Pb^{2+} ions. Probe **12** displayed a large shift in its absorption band, *i.e.*, 110 nm, upon the addition of Ni^{2+} and Cd^{2+} ions with a change in the color of the probe solution from red to blue (visible to the naked eyes), together with two clear isosbestic points. The Job's plot analysis further indicated a 2 : 1 binding ratio for Ni^{2+} and Cd^{2+} with the association constant values of 1.4×10^{10} M^{-2} and 4.8×10^{9} M^{-2} and the limit of detection (LoD) of 8.7×10^{-7} M and 2.8×10^{-6} M, respectively. Zn^{2+} and Pb^{2+} showed distinctive spectral changes but no color change was observed in these cases. The emission of probe **12** was suppressed due to the presence of triazole and ferrocene units (ϕ_{em} = 0.001); however, the addition of only Zn^{2+} resulted in a slight enhancement in its emission band (ϕ_{em} = 0.006). Electrospray ionization mass spectroscopic (ESI-MS) analysis of **12** in the presence of Ni^{2+} and Cd^{2+} exhibited 1 : 1 fragments with $[\mathbf{12}\text{-}CdClO_4]^+$ (*m*/*z* 803) and $[\mathbf{12}\text{-}NiClO_4]^+$ (*m*/*z* 747), respectively.

In the same year (2021), Hishimone *et al.*[122] reported Cd^{2+}-based probe **14** with a thiosemicarbazone group in the ligand framework (Fig. 12). In DMF solution, the UV-Vis studies for **14** revealed a high-intensity ILCT band centred at 410 nm together with a low-intensity MLCT band near 535 nm. A moderate-intensity absorption was also observed at 306 nm, which is most likely due to the LC $\pi \rightarrow \pi^*$ transition. The nitrate salts of cations such as Fe^{3+}, Ag^+, Zn^{2+}, Mn^{2+}, Cu^{2+}, Co^{2+}, Ni^{2+}, Cd^{2+}, Cr^{3+}, Pb^{2+} and Hg^{2+} were added to the probe solution, and the changes in its absorption spectrum were monitored. Upon the addition of Ni^{2+} ions (5.0 equiv.) to the probe solution (*ca.* 10^{-5} M) in DMF, the ILCT band at 410 nm decreased, and concomitantly a new band appeared near 500 nm, which suggested the formation of a new species. An isosbestic point was also observed at 437 nm with a substantial change in the color from yellow to brown (obvious to the naked eyes). Other metal ions such as Cu^{2+}, Co^{2+} and Hg^{2+} produced similar changes in the absorption spectra with a similar colorimetric response. The formation of adduct **14**-Ni^{2+} was also corroborated by ESI-MS and NMR analyses. No changes in the spectra were observed upon introducing anionic species such as F^-, OH^-, CN^-, AcO^-, Cl^-, Br^-, I^- and HSO_4^- ions. The binding constant and LoD values for **14**-Ni^{2+} were computed to be 1.55×10^2 M^{-1} and 1.30×10^{-10} M, respectively.

5. MOF-based sensors

Metal–organic frameworks (MOFs) are inorganic–organic hybrid materials typically assembled by metal ions/metal clusters and suitable organic ligands through coordinate bonds to form one-, two-, or three-dimensional structures.[123,124] The appropriate selection of organic compounds and metal ions plays a crucial role in the design and development of MOFs. Distinctively from traditional solid-state porous materials, *e.g.*, zeolites, molecular sieves and activated carbons, MOFs display some unique structural features mainly due to their open porous structure, remarkable porosity, large surface area, and tuneable pore surface.[125,126] These intrinsic characteristics have facilitated the application of MOFs in different fields including gas adsorption/separation,[127,128] magnetic materials,[129,130] drug delivery,[131,132] heterogeneous catalysis,[133,134] and optical devices.[135,136] Amongst them, the use of MOFs as luminescent or colorimetric sensing materials to detect various analytes (such as cations, anions, and neutral molecules) constitutes one of the most important applications. Hence, over the years, a diverse panel of luminescent MOF-based probes have been developed to detect metal ions, anions, small gases, organic molecules, *etc.*,[137–139] while MOFs substantially acting as colorimetric sensors are relatively less explored.

The following section only covers MOFs acting as optical probes specifically for the detection of Ni^{2+} ions. Thus far, most of the studies on MOFs as luminescent probes for detecting Ni^{2+} have been mainly related to Zn^{2+}- and Cd^{2+}-based metallic cores. More recently, MOFs involving lanthanide ions have also emerged as an intriguing alternative in the sensing field.

5.1 Luminescent Ni^{2+} sensors

In 2015, Wang *et al.*[140] reported cadmium-based MOF **15** as a luminescent probe to detect Ni^{2+} in *N*,*N*′-dimethylacetamide (DMA) solution. Probe **15** was comprised of non-interpenetrating pillar-layers bearing 5-aminoisophthalic acid and 3,5-(dipyridin-4-yl)-4*H*-1,2,4-triazol-4-amine groups as organic ligands. Recently, pillar-layer MOFs have attracted significant attention from researchers due to their following key features: (i) a variation in the length of the pillar linkers may tune the shape and size of the pores with a negligible change in the structural topology of the MOF and (ii) the direct functionalization of the pillar linkers may result in a variation in the hydrogen bonding and hydrophobic/hydrophilic character of the MOF. Accordingly, 3,5-(dipyridin-4-yl)-4*H*-1,2,4-triazol-4-amine was chosen as the organic linker due to its extended π-conjugated feature to improve the luminescent character of the resultant MOF. Moreover, the Cd^{2+} ion was selected to construct the metallic core in probe **15** due to its multiple coordination numbers and promising photophysical properties. A pentagonal bi-pyramidal geometry was adopted by Cd^{2+} bearing five oxygen atoms at the equatorial positions and two nitrogen atoms at the axial positions (Fig. 13). To determine its sensing ability for cations, a DMA solution of different metal salts, *e.g.*, Cd^{2+}, Co^{2+}, Ag^{+}, Ni^{2+} and Zn^{2+} (*ca.* 10^{-2} M) was individually introduced in a DMA solution of probe **15**. A luminescence enhancement in the intensity of **15** at 410 nm could be realized in the case of Cd^{2+}, Zn^{2+} and Ag^{+}, most likely due to their closed-shell electronic configuration. In contrast, Co^{2+} and Ni^{2+} induced luminescence quenching with the most significant decline in the case of Ni^{2+}. The largest enhancement (*ca.* 8.0-fold) observed for Cd^{2+} was attributed to the bridging effect, which enhances the conjugation and the rigidity of the probe, while the quenching in the case of Ni^{2+} was ascribed to the reduction in the intraligand luminescence efficiency *via* weak binding between Ni^{2+} and the nitrogen atoms.

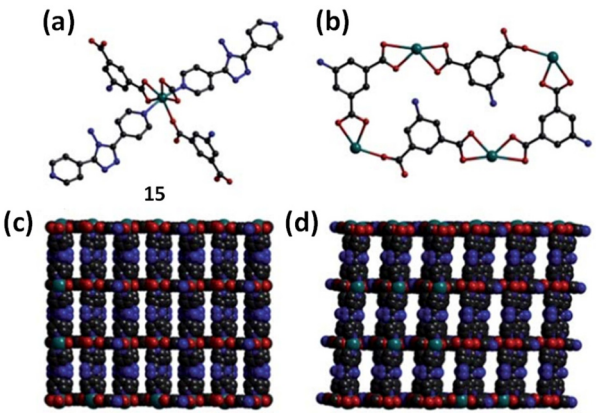

Fig. 13 (a) Coordination environment of cadmium centre in probe **15** [Cd, teal; C, black; O, red; and N, blue] and (b) macrometallocycles. (c) & (d) Channel representation of probe **15**. Adapted with permission from ref. 140. Copyright 2015, The Royal Society of Chemistry.

In the same year, another Cd^{2+}-based probe, **16**, was synthesized by Feng and co-workers[141] for the recognition of Ni^{2+} in aqueous solution. The 5-(4-carboxybenzyloxy)-isophthalic acid ligand was chosen as the bridging group due to the presence of three carboxylate ($-COO^{-}$) moieties in this ligand, which may ultimately lead to diverse bridging modes to be adopted in the construction of the MOF. The solid-state luminescence behavior of **16** was investigated at room temperature. The emission maximum was observed near 443 nm when excited at 368 nm and was attributed to the ligand-to-metal-charge-transfer (LMCT) transition. The luminescence sensing ability of **16** for different metal ions such as K^{+}, Co^{2+}, Ni^{2+}, Zn^{2+}, Cu^{2+}, Ba^{2+} and Pb^{2+} was studied in aqueous solutions. Quenching of the emission band at 443 nm was observed in the case of Cu^{2+}, Ba^{2+}, Co^{2+}, Zn^{2+} and Ni^{2+}, with the most significant effect for Ni^{2+}, which is most probably due to the strong coordination of Ni^{2+} with the free carboxylate moieties.

In lanthanide chemistry, the Ln(III) f–f transitions are Laporte forbidden, typically resulting in low absorption coefficients, and thus the photophysical characteristics of Ln(III) are dependent on the coordinating environment of Ln(III). Thus, to overcome this inherent obstacle, an appropriate organic ligand displaying the 'antenna effect' (*vide supra*) is usually incorporated in the Ln(III) centre.[142–144] An alternative to improve the emission of Ln(III) is to incorporate a d-block metal complex (transition metal complex) as sensitizer for the lanthanide emission. To engineer the latter, a suitable organic ligand is typically chosen to bridge the d-block metal-based chromophore and the Ln(III)-based luminophore into d–f heterobimetallic species. Subsequently, the sensitized luminescence of the Ln(III) is achieved *via* d → f energy transfer. The d-block chromophore employed with Ln(III) may enhance or quench the luminescence of Ln(III), relying on either d → f or f → d energy transfer, respectively.[145–147] However, most of the works reported thus far are limited to the development of bimetallic 3d–4f, 4d–4f or 5d–4f species.

To further extend this concept, in their elegant study, Wang *et al.*[148] developed two structurally similar Yb(III)–Cd(II)–Mn(III)- and Yb(III)–Cd(II)–Zn(II)-based luminescent MOFs **17** and **18** bearing oxidiacetic acid as the ligand, respectively (Fig. 14). This was the first report representing a mixed 4f–4d–3d framework exhibiting selectivity towards Ni^{2+} ions. The authors anticipated that the direct interaction of the 3d or 4d orbitals of transition metal ions with the 4f orbital of Yb(III) may tune the energy of the 4f level, resulting in a variation in the luminescence performance of Yb(III). After excitation at 360 nm, a narrow sharp band was observed between 975 nm and 1025 nm with the emission maximum centred at 998 nm

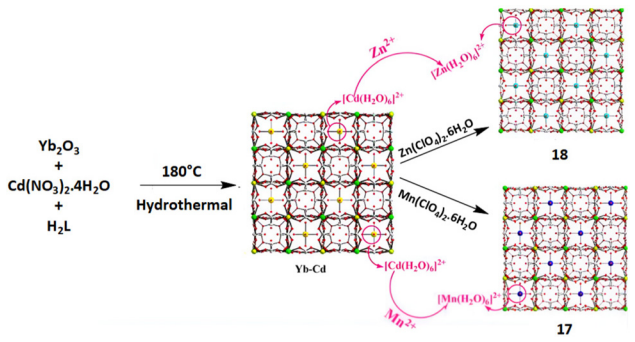

Fig. 14 Synthesis of trimetallic MOF probes **17** and **18**. Adapted with permission from ref. 149. Copyright 2015, American Chemical Society.

in DMF solution. This emission band was assigned to the Yb (III)-based $^2F_{5/2} \rightarrow {}^2F_{7/2}$ transition. Probe **17** exhibited a luminescence quenching response at 995 nm in the presence of Ca^{2+}, Mg^{2+}, Ni^{2+} or Zn^{2+} and drastic quenching could be observed in the case of Cd^{2+} or Co^{2+} in DMF solution. Conversely, probe **18** showed a remarkable luminescence enhancement at 998 nm when Ni^{2+} ions were added to it, while the intensity of this peak was diminished in the presence of Ca^{2+}, Co^{2+} and Mg^{2+} ions. The luminescence enhancement was attributed to the changes in the excited-state level of the Cd^{2+} moiety, which transferred energy more efficiently to the Yb^{3+} ions.

In 2016, a series of isostructural Ln(III)-based 1D polymeric materials equipped with tetrafluorophthalic acid and 1,10-phenanthroline as ligands was demonstrated by Li and group.[149] Among the different Ln(III) ions including Sm(III), Eu(III), Gd (III), Tb(III) and Dy(III), only probe **19** involving Eu(III) was reported to have selectivity towards nitrobenzene and Ni^{2+} ion. The characteristic emission bands for Eu^{3+} were observed at 594 nm, 614 nm, 651 nm and 683 nm due to the $^5D_0 \rightarrow {}^7F_J$ transitions (where J = 1–4). The strongest transition, *i.e.*, $^5D_0 \rightarrow {}^7F_2$, was attributed to the electronic dipole transition, which is responsible for the characteristic red color of Eu^{3+}. This probe displayed a luminescence lifetime of 0.5565 ms with an emission quantum yield of 15.87%. A suspension was observed after the dispersion of **19** in an aqueous solution of various metal ions. A variable degree of emission quenching was exhibited by Na^+, Cd^{2+}, K^+, Li^+, Al^{3+}, Ca^{2+} and Ni^{2+}, whereas Mg^{2+} and Pb^{2+} ions caused a slight change in the emission. The most pronounced effect was noticed in the case of Ni^{2+}, where 1.0 mmol L^{-1} Ni^{2+} ions induced significant emission quenching (*ca.* 90%) at 615 nm. Upon the progressive addition of Ni^{2+} (up to 10.0 mmol L^{-1}) to **19**, its emission band was almost completely quenched (approx. 99%). This quenching behavior was attributed to the partially filled d-subshell of the target ions. This MOF was also robust enough and showed identical results for Ni^{2+} and nitrobenzene even after five cycles.

In the same year (2017), Zheng *et al.*[50] presented a series of Ln-MOFs with 1,3-adamantanediacetic acid and 1,10-phenanthroline as ligands. Probe **20** having Eu as the metallic core exhibited the characteristic emission bands for the Eu^{3+} ion at 576 nm, 592 nm, 613 nm, 650 nm, and 698 nm, corresponding to the $^5D_0 \rightarrow {}^7F_J$ (J = 0 to 4) transitions, respectively. The lifetime of probe **20** was reported to be 1.478 ms with a quantum yield of 58.61%. Interestingly, the Tb^{3+} analogue of probe **20** displayed a much lower quantum yield (9.07%), which suggested that the phen moiety transfers energy more preferably to the Eu^{3+} ion than to the Tb^{3+} ion. Probe **20** exhibited luminescence quenching in the presence of Ni^{2+} in water, while other metal ions such as Mn^{2+}, Co^{2+}, Cd^{2+}, Ba^{2+}, Zn^{2+}, Pb^{2+}, Cr^{3+}, Fe^{2+} and Mg^{2+} resulted in negligible changes in its emission spectrum. Moreover, among the different amino acids tested, the addition of valine resulted in drastic enhancement in the emission intensity of **20**. This probe had a low LoD value of 1×10^{-9} M; however, a significant interference was experienced from Cd^{2+}, Mg^{2+}, Co^{2+}, Mn^{2+}, Val and Trp. The quenching mechanism was explained based on the LMCT after the addition of Ni^{2+} ions, which interrupts the antenna effect. The other analogues of **20** with Gd^{3+}, Tb^{3+}, La^{3+}, Ce^{3+}, Pr^{3+}, Nd^{3+}, and Y^{3+} displayed no selectivity or sensitivity to Ni^{2+} ions. Later, in 2018, Wu and co-workers[150] developed luminescent probe **21**, a cyclopentanedicarboxylic acid and Zn^{2+}-based coordination polymer. The narrow emission maximum of **21** was observed at 584 nm in phosphate buffered saline (PBS) solution. This probe showed a high degree of quenching upon the addition of Ni^{2+} ions, while other ionic species such as Al^{3+}, Ca^{2+}, Cd^{2+}, Co^{2+}, Mg^{2+}, Mn^{3+}, Pd^{2+}, Zn^{2+}, Na^+, K^+, NH_4^+, NO_3^-, and Cl^- failed to cause any changes in its emission intensity. Slight quenching was also observed in the case of Fe^{3+} and Cu^{2+} but the response was nominal in comparison to that for Ni^{2+}. Metal ions such as Fe^{3+} and Cu^{2+} ions did not interfere in the selective detection of Ni^{2+} ions, which is a key parameter to utilise **21** for practical applications in real specimens. The influence of temperature and pH on the luminescence behavior of this probe was also studied. The authors reported that the optimal pH was in the range of 4.0–6.0, and the luminescence intensity was reduced by 34.5% when the temperature was increased from 25 °C to 50 °C. Probe **21** was also tested in real samples such as filtered lake water using PBS buffer solution (pH 7.0). Six different samples were taken from the Songshan Lake. Initially, the solutions were filtered to remove any insoluble earthy bulk materials, followed by the addition of PBS buffer to maintain the pH of 7.0. The excellent recoveries of 99% to 104% with the relative standard deviation of 3.0% suggested the potential utility of this MOF as a chemosensory probe in environmental settings. The Stern–Volmer constant of 5.74×10^5 L mol^{-1} with a bimolecular quenching constant of 5.47×10^{13} L mol^{-1} s^{-1} indicated a static quenching mechanism and a remarkable soft acid–base interaction between Ni^{2+} and carbonyl groups. The LoD value for Ni^{2+} was calculated to be 5.23×10^{-7} mol L^{-1} in this study.

Later, Cu^{2+}-based MOF **22** containing 2-aminobenzene-1,3,5-tricarboxylate as the organic linker was designed by Rubin *et al.* in 2019 (Fig. 15(a)).[151] The emission spectrum of **22** displayed a band near 400 nm in DMF solution. To investigate the sensing behavior of **22** for different cations, a 10 mM solution of various metal ions was added to 2 mg of finely dis-

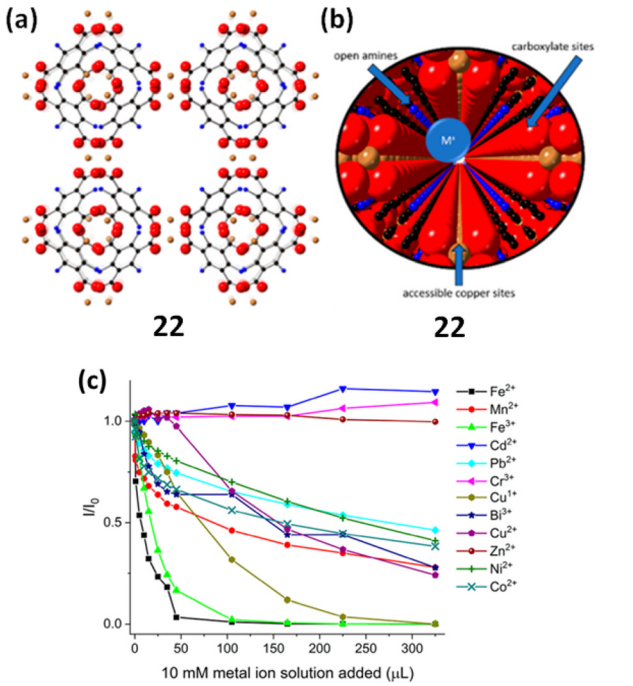

Fig. 15 (a) Secondary-building-unit (SBU) of probe **22** having available functionalities such as amines (in blue color), carbon (in black color), oxygen (in red color) and Cu (in tan color). (b) Space-filling model exhibiting the possible interaction site for the guest metal ion in the framework and (c) normalized emission intensity (I/I_0, where λ_{em} = 400 nm and λ_{ex} = 350 nm) of probe **22** in the presence of 10 mM of different metal ions. Adapted with permission from ref. 151. Copyright 2019, the American Chemical Society.

persed **22** in DMF, which was shaken for 30 s and sonicated for 1 h. The emission spectrum of **22** exhibited complete quenching upon the progressive addition of Fe^{2+} and Fe^{3+} (1.55 to 56.0 ppm). Noticeable quenching was also reported for Pb^{2+}, Cu^{2+}, Mn^{2+}, Ni^{2+} and Co^{2+} with a detection limit of 5.7, 12.0, 3.0, 1.6 and 0.2 ppm, respectively (Fig. 15(c)). Also, **22** was found to be sensitive to anions such as CO_3^{2-}, AcO^- and $Cr_2O_7^{2-}$, whereas other common anions such as Cl^-, Br^-, I^- and NO_3^- caused nominal changes. The diverse sensing behavior of this MOF was demonstrated by the HSAB theory. According to the HSAB principle, the luminescence quenching was observed by either borderline hard acids, *e.g.*, Bi^{3+}, or soft acids such as Cu^+, whereas the hard acids, *e.g.*, Cr^{3+}, showed no remarkable change in emission intensity. Furthermore, alkali metals showed a nominal change in the spectrum, whereas alkaline earth metals exhibited *ca.* 50% luminescence quenching with the appearance of a new peak at 475 nm. The authors anticipated that the interaction of a molecule in the excited-state with a nearby non-excited molecule may lead to the changes observed in the luminescence profiles. The reason for the observed luminescence quenching was attributed to the blockage of the free amine group induced by the guest analyte in the probe.

In the subsequent year (2020), Qin *et al.*[51] synthesized highly luminescent probe **23**, a Zn^{2+}-based MOF bearing 4,4′-oxybis-(benzoic acid) and 4-amino-3,5-bis(4-pyridyl)-1,2,4-triazole as the organic linkers. Three metal centres were linked by the SO_4^{2-} ion to give a tri-metallic node acting as a secondary building unit (SBU) in probe **23**. Finally, a 2D tripillared-bilayer structure could be obtained *via* the linking between the SBU and the ligands. The emission spectrum of **23** showed an intense band near 474 nm when excited at 310 nm. To investigate the cation sensing ability of **23**, it was soaked in a 10 mM aqueous solution of different metal ions such as Na^+, K^+, Mg^{2+}, Al^{3+}, Pb^{2+}, Co^{2+}, Ni^{2+}, Cd^{2+}, Zn^{2+}, Mn^{2+} and Cr^{3+}. Subsequently, the guest-containing solutions were filtered and dried and their luminescence spectra recorded. Among the various metal ions tested, Ni^{2+} caused the strongest luminescence quenching (*ca.* 93%) with a slight enhancement in the case of K^+, Zn^{2+} and Mg^{2+} ions. The quenching behavior of **23** towards Ni^{2+} was ascribed to the strong interaction of the Ni^{2+} ion with uncoordinated nitrogen and oxygen atoms accessible in the MOF. The K_{sv} value for Ni^{2+} was reported to be 98 127 M^{-1} with a detection limit of 0.46 μM. This probe was also found to be sensitive to PO_4^{3-} ions but with a relatively higher detection limit (approx. 6.5 μM) compared to Ni^{2+} ions.

During the same period, Peng *et al.*[152] reported Eu^{3+}-based MOF **24** bearing 1,2,4-benzene tricarboxylic acid, which acted as an antenna in the MOF. Probe **24** was prepared by the co-precipitation method, and its morphology could easily be adjusted from spherical to irregular honeycomb by simply changing the pH of the reaction medium. The characteristic emission bands of Eu^{3+} were observed near 591 nm, 617 nm and 702 nm due to the typical $^5D_0 \rightarrow {}^7F_1$, $^5D_0 \rightarrow {}^7F_2$, and $^5D_0 \rightarrow {}^7F_4$ transitions, respectively (λ_{ex} = 395 nm). The sensing ability of **24** was tested against Al^{3+}, Zn^{2+}, Na^+, Ca^{2+}, Sr^{2+}, Ba^{2+}, Mg^{2+}, Ni^{2+}, Cr^{3+}, Cu^{2+} and Fe^{3+} ions. Among them, only Fe^{3+}, Cr^{3+} and Ni^{2+} displayed considerable luminescence quenching, while no changes could be observed in the case of other metal ions. The luminescence quenching response in **24** was attributed to the 'ion-fence' effect, in which the target metal ion creates a fence surrounding the probe, ultimately interrupting the ligand-sensitized 'antenna effect'.

In the following year (2021), Guan and group[153] reported Al^{3+}-based MOF **25** incorporated with Eu^{3+} and 3,3′-diethyloxocarbocyanine iodide (or DOC) organic dye (Fig. 16(a)). This probe had three active luminescent centres, *i.e.*, parent Al^{3+}-MOF, Eu^{3+} and DOC, and tuneable luminescence behavior could be realized by systematically adjusting the content of either Eu^{3+} or DOC in the parent MOF. The characteristic Eu^{3+} bands were observed at 578 nm, 592 nm, 614 nm, 652 nm and 688 nm (due to $^5D_0 \rightarrow {}^7F_J$ transitions, where J = 0–4) when excited at 350 nm, respectively. The energy transfer efficiency from the ligand to Eu^{3+} could also be tuned by choosing a suitable excitation wavelength. For instance, upon excitation at 360 nm, the intense emission bands for Eu^{3+} and DOC and the organic ligand appeared near 614 nm, 520 nm and 420 nm, respectively (Fig. 16(b)). The luminescence sensor array, hence obtained, could identify Ag^+, Co^{2+}, Cu^{2+}, Fe^{3+} and Ni^{2+} by exhibiting variable luminescence quenching in the above-mentioned bands in aqueous medium (Fig. 16(c)).

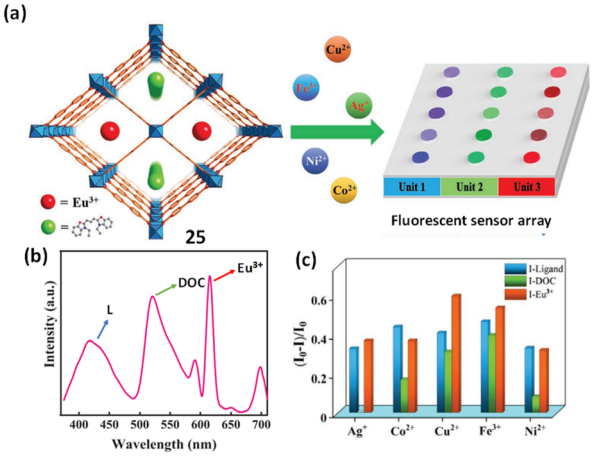

Fig. 16 (a) Construction of the MOF **25**-based sensor array; (b) emission spectrum of probe **25** and (c) luminescence response $[(I_0-I)/I_0]$ of three emitting centers in **25** toward Ag^+, Co^{2+}, Cu^{2+}, Fe^{3+} and Ni^{2+} ions. Adapted with permission from ref. 153. Copyright 2021, Wiley.

Moreover, LDA (linear discriminant analysis) was employed to differentiate between Ni^{2+} and Co^{2+}, which possess similar behaviour and size with a 5.33% misjudgement in 75 investigated samples. For potential future applications, the metal ion sensing ability of **25** was explored using lake water samples (West Lake), and the discrimination accuracy for individual metal ions (*ca.* 60 μM) was nearly 100%.

In the same year (2021), Perumal and co-workers[49] employed an interesting strategy for the selective sensing of multiple metal ions. Luminescent nickel-cobalt based MOF **26** equipped with MoS_2 (molybdenum disulfide) nano-box was developed as a biosensor to fabricate a Y-shaped DNAzyme for the multiple-detection of Ni^{2+}, Hg^{2+} and Ag^+ ions in real water samples (Fig. 17(a)). The DNAzyme produced three emission

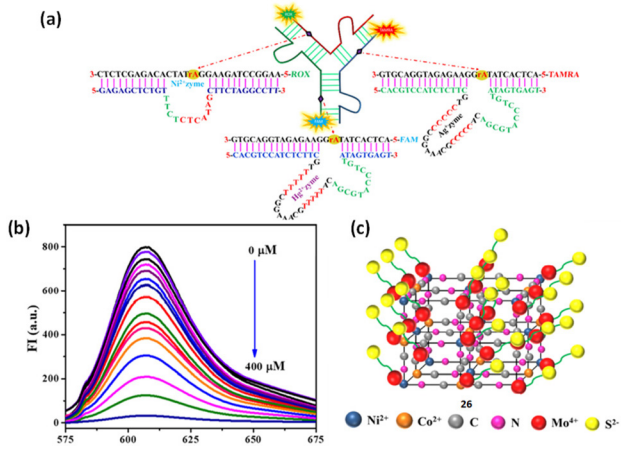

Fig. 17 (a) Structure of Y-shaped DNAzyme labeled with three fluorophores FAM, ROX and TAMRA; (b) fluorescent quenching in the emission band of **26** after the addition of 400 μM Ni^{2+} ions and (c) structure of probe **26**. Adapted with permission from ref. 49. Copyright 2021, American Chemical Society.

peaks centred at 523 nm, 606 nm and 572 nm in the absence of the target metal ions. The DNAzyme, labelled with three fluorophores FAM, ROX and TAMRA, displayed a weak binding affinity to the MOF. These fluorophores, acting as substrate aptamers, were cleaved by the interaction between the respective metal ion and the three enzyme aptamers. Therefore, the cleaved substrate aptamers were adsorbed on the surface of the MOF, which exhibited a turn-off response with the help of van der Waals or π–π stacking interactions. Hg^{2+} ions cleaved the aptamer FAM and coordinated with the thymine base pairs, whereas Ag^+ cleaved TAMRA to coordinate with the cytosine base pairs. The alteration of the RNA sites to carbonyl and imidazole functionalities assisted the detection of Ni^{2+} ions with the concomitant release of the ROX substrate aptamer. The response time of probe **26** was 5.0 min with an optimum pH of 8.0. The sensing of Ag^+, Ni^{2+}, and Hg^{2+} was not affected by the presence of other metal ions such as Zn^{2+}, Co^{2+}, Mg^{2+}, Pb^{2+}, K^+, Cd^{2+}, Cu^{2+}, Ba^{2+}, Fe^{3+}, Mn^{2+}, Cr^{3+}, Ca^{2+} and Cr^{6+}. The LoD values for Hg^{2+}, Ni^{2+} and Ag^+ ions were calculated to be 0.11, 7.8 and 0.25 nM, respectively. Probe **26** was also able to detect metal ions in spiked lake and tap water samples with an excellent recovery value in the range of 99–103.5%. Initially, the pH of the samples was adjusted to 8.0 using 10 mM Tris-HCl buffer and the diluted samples were spiked with Ni^{2+} ions. The detection results were also reproducible with an RSD value of 3.4%. A similar set of experiments was also performed for Ag^+ and Hg^{2+} ions, suggesting the potential utility of **26** in environmental cation monitoring applications.

Recently, Kabak *et al.* synthesized an Eu^{3+}-based MOF **27**[154] using the solvothermal method with 1,4-benzenedicarboxylic acid, 1,10-phenanthroline, and *N*,*N*′-dimethylformamide as binding units. When excited at 254 nm, **27** exhibited its characteristic emission band at 615 nm due to the $^5D_0 \rightarrow {}^7F_2$ transition. The luminescence of **27** was quenched with Cu^{2+}, Ni^{2+}, and T3, T4 species, while metal ions such as Al^{3+}, Mn^{2+}, Cr^{3+}, Mg^{2+}, Pb^{2+}, Ca^{2+}, Hg^{2+}, Na^+, Fe^{3+} and K^+ showed negligible changes in water. The Stern–Volmer quenching constant was reported to be 3.19×10^7 M^{-1} with an LoD of 1.47 μM. This probe was found to be capable of detecting Ni^{2+} ions in drinking and tap water samples in the μM range. The recovery range of **27** (94–102.3%) clearly indicated that this probe can find future application in both *in vitro* and *in vivo* studies.

Mei and Yan (2023)[155] developed probe **28**, a zeolitic imidazole framework including 4-aminobenzoic acid, Eu^{3+} ions, and flumequine for the detection of cations in different water sources (such as deionized water, drinking water and nuclear wastewater). The emission spectrum of **28** revealed five emission bands at 578 nm, 596 nm, 616 nm, 652 nm and 700 nm (due to $^5D_0 \rightarrow {}^7F_J$ transitions; J = 0–4) when excited at 348 nm, respectively. The flumequine is essential to sensitize Eu^{3+} due to the fact that its T1 level (19 230 cm^{-1}) is close to that of Eu^{3+} (17 500 cm^{-1}), which facilitates efficient energy transfer. Among the investigated metal ions such as Na^+, K^+, Li^+, Ag^+, Mg^{2+}, Ca^{2+}, Zn^{2+}, Sr^{2+}, Ba^{2+}, Pb^{2+}, Hg^{2+}, Mn^{2+}, Ln^{3+}, Ni^{2+}, Cu^{2+} and UO_2^{2+}, probe **28** exhibited quenching with Ni^{2+}, Cu^{2+}, and UO_2^{2+} ions. Furthermore, the addition of $NaHCO_3$ resulted in

the reappearance of the fluorescence band at 616 nm for UO_2^{2+}; however, no change was reported in the case of Ni^{2+} and Cu^{2+}. The LoD values for Ni^{2+}, Cu^{2+}, and UO_2^{2+} were reported to be 1.3×10^{-2}, 6.1×10^{-4}, and 9×10^{-3} ppm, respectively. The sensing ability of **28** for Ni^{2+} was also assessed in real drinking water (Tongji University). The addition of Ni^{2+} resulted in the quenching of its emission band; however, the sensitivity in drinking water was lower (2.8×10^{-2} ppm) in comparison to deionized water. Nonetheless, **28** still exhibited a lower LoD than the concentration defined by the EPA. The sensing mechanism was investigated by luminescent lifetime studies, where it was seen that the luminescent lifetime decreased in the case of Ni^{2+} and Cu^{2+} ions; however, the lifetime was not affected in the presence UO_2^{2+} ions. This result suggested that Ni^{2+} and Cu^{2+} follow dynamic quenching, whereas UO_2^{2+} exhibits static quenching. Moreover, the absorption band of UO_2^{2+} overlapped with the excitation spectra of the probe, which supported competitive absorption between the probe and the analyte. The DFT studies revealed that the binding of Ni^{2+} and Cu^{2+} has a large binding energy and chelation causes electron transfer to the metal ion, which suggested PET as the possible mechanism.

5.2 Chromofluorogenic Ni^{2+} sensors

In 2015, Nd^{3+}-based luminescent MOF **29** having bis-dithiocarbamate as an organic linker was synthesized by Xu *et al.*[156] for the chromofluorogenic recognition of Ni^{2+} ions. Probe **29** was found to be stable in methanol but relatively less stable in aqueous media. Three sharp emission bands could be observed in the NIR region at 903 nm, 1077 nm and 1364 nm due to the Nd^{3+}-centred transitions, *i.e.*, $^4F_{3/2} \rightarrow {}^4I_{9/2}$, $^4F_{3/2} \rightarrow {}^4I_{11/2}$ and $^4F_{3/2} \rightarrow {}^4I_{13/2}$, respectively. The 1D channel and architectural stability of **29** led the authors to assess its ion exchange behavior. The cation exchange experiment was studied *via* 10 min immersion of fresh crystals of **29** in a methanolic solution containing the target metal ions. The crystal structure of **29** was stable only with Ni^{2+}, whereas in the presence of other cations the crystals collapsed. The emission intensity of the band at 1077 nm significantly decreased upon the gradual addition of Ni^{2+}, and the latter was coupled with a change in color of the crystal from light grey to olive (Fig. 18(d)). The quenching constant was computed to be 84.89 M^{-1}, and the quenching mechanism was ascribed to a combination of dynamic and static quenching processes. The authors suggested that the dynamic quenching may be governed by the collisions existing between the ligand and Ni^{2+}, while simultaneously the static quenching mechanism may occur due to the interactions existing between the S groups of the ligand and the Ni^{2+} ion.

In 2017, Sun's group[157] synthesized heterobimetallic MOF (4d–4f species) **30** containing 4-(4-pyridinyl)-benzoic acid and 2-methyl-1*H*-4,5-imidazole-dicarboxylic acid as organic linkers (Fig. 19(a)). The 4f element employed to construct the MOF was Eu, whereas Cd metal was chosen from the 4d series. Probe **30** displayed an excellent luminescent property, and therefore employed for the detection of different metal ions.

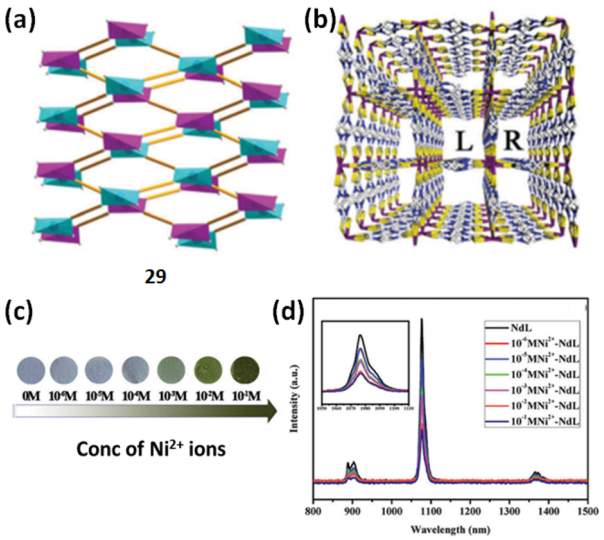

Fig. 18 (a) Interpretation of 1d channel of Nd-based MOF **29**. (b) Channel enclosed by R-helices and L-helices. (c) Probe **29** after immersion in Ni^{2+} solution and (d) changes in its emission spectrum in the presence of different Ni^{2+} concentrations. Adapted with permission from ref. 156. Copyright 2015, The Royal Society of Chemistry.

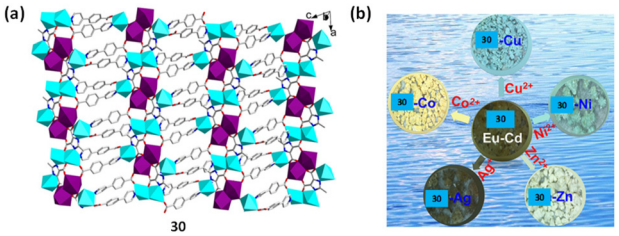

Fig. 19 (a) 2D polyhedral view of probe **30** (colors: Eu = purple, Cd = cyan, O = red, N = blue, and C = gray) and (b) crystal photograph of **30** dispersed in aqueous metal solution. Adapted with permission from ref. 157. Copyright 2017, American Chemical Society.

The emission spectrum of **30** displayed three characteristic bands at 592 nm, 617 nm and 686 nm, typically due to the $^5D_0 \rightarrow {}^7F_1$, $^5D_0 \rightarrow {}^7F_2$, and $^5D_0 \rightarrow {}^7F_4$ transitions, respectively. The emission decay lifetime of this MOF was 673 μs, which was fitted by a double-exponential curve. Owing to the presence of carboxylic groups, the luminescence response of **30** was tested against many cations, organic solvents, and organic amine molecules. The powdered MOF was immersed in 0.1 M aqueous solutions of K^+, Er^{3+}, Li^+, Na^+, Ca^{2+}, Ag^+, Mg^{2+}, Zn^{2+}, Cd^{2+}, Ba^{2+}, Pb^{2+}, Al^{3+}, Cu^{2+}, Co^{2+}, Cr^{3+}, Fe^{3+} and Ni^{2+} to monitor the changes observed in the emission spectrum of **30**. The Mg^{2+} ion caused a significant enhancement in the luminescence intensity of **30**. Alternatively, an emission quenching response was observed in the case of Co^{2+}, Ni^{2+}, Cu^{2+}, Zn^{2+} and Ag^+ ions. The probe was sensitive to the metal ions in the order of $Cu^{2+} > Ag^+ \approx Co^{2+} \approx Ni^{2+} \approx Zn^{2+}$. The color change to blue, green, light yellow, dark brown and yellow was obvious, respectively, for Cu^{2+}, Ni^{2+}, Zn^{2+}, Ag^+ and Co^{2+} ions (Fig. 19(b)).

The PXRD patterns for the probe and the probe-cation adduct were similar, which confirmed the stability of the framework. The cations concurrently competed when the probe was excited, which resulted in the luminescence quenching. The interaction between the uncoordinated carboxylate and target ion altered the energy of singlet- and triplet- excited states, leading to the inhibition of the 'antenna effect' with a simultaneous reduction in the energy transfer from the ligand to the Eu(III) ion.

6. Conclusions

The present review highlighted the optical detection of Ni^{2+} using metal complexes and MOFs as receptors. Although this review covered the detection of only Ni^{2+}, a total of 30 metal–organic probes was discussed, signifying the importance of this research field. As observed from the summarized examples, the luminescent/colorimetric sensing of nickel ions substantially relies on the binding-based approach, while interacting with metal complexes and/or MOFs. The extent of the interaction between nickel ion and the binding unit depends on both the nature of the target ion, *i.e.*, Ni(II), and the donor groups incorporated in the receptor. Therefore, the significance of Pearson's HSAB (hard and soft acid and base) principle emphasizing the role of different donor atoms has been consistently highlighted, which is a key feature for a highly selective and sensitive detection process.

Beyond their advantageous design flexibility and their conspicuous properties (notably compared to their organic counterparts), the consideration of metal complexes as receptors also implies several distinct mechanisms to propitiously design luminescent and colorimetric molecular probes. Among these rationales, PeT is recurrently reported as the typical mechanism for cation-responsive luminescent probes, while the intramolecular charge transfer (*i.e.*, ICT) process is usually assessed for colorimetric probes. However, despite their significance in sensing, it has been realized that several metal complexes display a lack of selectivity for the detection of Ni^{2+} in presence of Cu^{2+}. These observations further cement the vital aspect of the judicious choice of donor groups in receptors to achieve the highly selective sensing of a specific metal ion.

In case of MOFs, the presence of N- and O-containing groups was found to be very important for the detection of Ni^{2+} ions; however, Co^{2+} acts as the major interfering species due to its competitive ionic radius and borderline acid character similar to that Ni^{2+}. However, despite the significant research devoted to cation-responsive MOF-based probes, their successful industrial implementation is still limited. This is attributed to the insufficient or missing stability/solubility of several MOFs in pure water. Therefore, the development of water-stable MOF receptors remains in high demand in modern research. In many cases, poor water solubility and mechanical strength are recurring disadvantages of MOFs, restraining their practical applications in various research fields. The water solubility of MOFs can also be improved by employing suitable linker groups such as triazolates, imidazolates and tetrazolates in the ligand framework.[158,159] Recently, the development of magnetic MOF (MMOF) composites has been attracting increasing attention from researchers in the sensing field due to their easy separation and reusability features.[130]

Also, near-*infra*-red (NIR)-active probes (optical window: 690–900 nm) should be emphasized. Alternatively, with respect to sustainability, the relative complexity of some sensing materials coupled with their unsatisfactory synthesis (*e.g.*, low yields, tedious synthesis or purification steps, and high costs) may harm the environment, humans and living beings in general. Therefore, with the support of green chemistry, environment-friendly synthetic strategies are urgently required to be adopted for future sensing materials. An alternative way is to design and develop recyclable and degradable sensors, which may help reduce environmental pollution on a large scale.[160,161] We hope that the significant collection of Ni^{2+} sensing probes compiled in this review will help build further comparative systematic SAR screenings and mechanistic investigations for the design of competitive sensors, which is the imperative first step before considering subsequent adequate solutions or treatments to the drawbacks of their overuse/mishandling.

Data availability

Data are available on request from the authors.

Conflicts of interest

There are no conflicts to declare.

Acknowledgements

SK acknowledges DST, New Delhi for INSPIRE Research Grant (IFA15/CH-213). The authors acknowledge the support received from CIC and Applied Science Cluster, UPES, Dehradun India. SN is grateful to UPES for financial support in terms of fellowship.

References

1 S. McCarthy, D. C. Braddock and J. D. E. T. Wilton-Ely, Strategies for sustainable palladium catalysis, *Coord. Chem. Rev.*, 2021, **442**, 213925.
2 I. Eryazici, C. N. Moorefield and G. R. Newkome, Square-planar Pd(II), Pt(II), and Au(III) terpyridine complexes: Their syntheses, physical properties, supramolecular constructs, and biomedical activities, *Chem. Rev.*, 2008, **108**, 1834–1895.
3 R. R. Panicker and A. Sivaramakrishna, Remarkably flexible 2,2′:6′,2″-terpyridines and their group 8–10 transition

metal complexes – Chemistry and applications, *Coord. Chem. Rev.*, 2022, **459**, 214426.
4 W. Zhu and T. B. Gunnoe, Advances in group 10 transition-metal-catalyzed arene alkylation and alkenylation, *J. Am. Chem. Soc.*, 2021, **143**, 6746–6766.
5 S. J. Firsan, V. Sivakumar and T. J. Colacot, Emerging trends in cross-coupling: Twelve-electron-based L_1 Pd(0) catalysts, their mechanism of action, and selected applications, *Chem. Rev.*, 2022, **122**, 16983–17027.
6 E. P. Broering, P. T. Truong, E. M. Gale and T. C. Harrop, Synthetic analogues of nickel superoxide dismutase: A new role for nickel in biology, *Biochemistry*, 2013, **52**, 4–18.
7 R. G. Kenny and C. J. Marmion, Toward multi-targeted platinum and ruthenium drugs - a new paradigm in cancer drug treatment regimens?, *Chem. Rev.*, 2019, **119**, 1058–1137.
8 A. D. Marchese, T. Adrianov and M. Lautens, Recent strategies for carbon–halogen bond formation using nickel, *Angew. Chem., Int. Ed.*, 2021, **60**, 16750–16762.
9 X. Zeng, C. Zhan, J. Lu and K. Amine, Stabilization of a high-capacity and high-power nickel-based cathode for Li-Ion batteries, *Chem*, 2018, **4**, 690–704.
10 D. Ulutan and T. Ozel, Machining induced surface integrity in titanium and nickel alloys: A review, *Int. J. Mach. Tools Manuf.*, 2011, **51**, 250–280.
11 M. Fanelli, M. Formica, V. Fusi, L. Giorgi, M. Micheloni and P. Paoli, New trends in platinum and palladium complexes as antineoplastic agents, *Coord. Chem. Rev.*, 2016, **310**, 41–79.
12 Y. Gou, G. J. Huang, J. Li, F. Yang and H. Liang, Versatile delivery systems for non-platinum metal-based anticancer therapeutic agents, *Coord. Chem. Rev.*, 2021, **441**, 213975.
13 X. Zhang, L. Li, E. Fan, Q. Xue, Y. Bian, F. Wu and R. Chen, Toward sustainable and systematic recycling of spent rechargeable batteries, *Chem. Soc. Rev.*, 2018, **47**, 7239–7302.
14 Y. Tang, W. Guo and R. Zou, Nickel-based bimetallic battery-type materials for asymmetric supercapacitors, *Coord. Chem. Rev.*, 2022, **451**, 214242.
15 V. K. Jain, Cyclometalated group-16 compounds of palladium and platinum: Challenges and opportunities, *Coord. Chem. Rev.*, 2021, **427**, 213546.
16 T. S. Lobana, Heterocyclic-2-thione derivatives of group 10–12 metals: Coordination versatility, activation of CS (thione) bonds and biochemical potential, *Coord. Chem. Rev.*, 2021, **441**, 213884.
17 A. Kumar, D. K. Jigyasu, A. Kumar, G. Subrahmanyam, R. Mondal, A. A. Shabnam, M. M. S. Cabral-Pinto, S. K. Malyan, A. K. Chaturvedi, D. K. Gupta, R. K. Fagodiya, S. A. Khan and A. Bhatia, Nickel in terrestrial biota: Comprehensive review on contamination, toxicity, tolerance and its remediation approaches, *Chemosphere*, 2021, **275**, 129996.
18 R. Balamurugan, J. H. Liu and B. T. Liu, A review of recent developments in fluorescent sensors for the selective detection of palladium ions, *Coord. Chem. Rev.*, 2018, **376**, 196–224.
19 K. Ravindra, L. Bencs and R. Van Grieken, Platinum group elements in the environment and their health risk, *Sci. Total Environ.*, 2004, **318**, 1–43.
20 L. Savignan, S. Faucher, P. Chéry and G. Lespes, Platinum group elements contamination in soils: Review of the current state, *Chemosphere*, 2021, **271**, 129571.
21 J. Aaseth, G. Crisponi and O. Anderson, *Chelation therapy in the treatment of metal intoxication*, Academic Press, 2016.
22 S. J. S. Flora and V. Pachauri, Chelation in metal intoxication, *Int. J. Environ. Res. Public Health*, 2010, **7**, 2745–2788.
23 W. Kerbib, S. Singh, D. Nautiyal, A. Kumar and S. Kumar, Ni(II) complexes of tripodal N4 ligands as catalysts for alkane hydroxylation and O-arylation of phenol: Structural and reactivity effects induced by fluoro substitution, *Inorg. Chim. Acta*, 2020, **517**, 120191.
24 N. Lalloo, C. E. Brigham and M. S. Sanford, Mechanism-driven development of group 10 metal-catalyzed decarbonylative coupling reactions, *Acc. Chem. Res.*, 2022, **55**, 3430–3444.
25 Y. Li and D. B. Zamble, Nickel homeostasis and nickel regulation: An overview, *Chem. Rev.*, 2009, **109**, 4617–4643.
26 S. B. Mulrooney and R. P. Hausinger, Nickel uptake and utilization by microorganisms, *FEMS Microbiol. Rev.*, 2003, **27**, 239–261.
27 H. Guo, H. Liu, Z. Jian, H. Cui, J. Fang, Z. Zuo, J. Deng, Y. Li, X. Wang, L. Zhao, R. He and H. Tang, Immunotoxicity of nickel: Pathological and toxicological effects, *Ecotoxicol. Environ. Saf.*, 2020, **203**, 111006.
28 I. Monograhs, Chromium, nickel and welding, *IARC Monogr. Eval. Carcinog. Risks Hum.*, 1990, **49**, 1–648.
29 World Health OrganizationNickel in drinking-water Background document for development of of WHO Guidelines for drinking-water quality. 2021 No. WHO/HEP/ECH/WSH/2021.
30 H. Zhang, Z. Liu, F. Xin and Y. Zhao, Metal-ligated pillararene materials: From chemosensors to multidimensional self-assembled architectures, *Coord. Chem. Rev.*, 2020, **420**, 213425.
31 Y. Fang and W. Dehaen, Small-molecule-based fluorescent probes for f-block metal ions: A new frontier in chemosensors, *Coord. Chem. Rev.*, 2021, **427**, 213524.
32 I. Narin, M. Soylak, L. Elçi and M. Doğan, Determination of trace metal ions by AAS in natural water samples after preconcentration of pyrocatechol violet complexes on an activated carbon column, *Talanta*, 2000, **52**, 1041–1046.
33 J. W. Olesik, Capillary electrophoresis for elemental speciation studies, *Compr. Anal. Chem.*, 2000, **33**, 151–211.
34 C. Jia, Y. Luo and J. Pawliszyn, Solid phase microextraction combined with HPLC for determination of metal ions using crown ether as selective extracting reagent, *J. Microcolumn Sep.*, 1998, **10**, 167–173.

35 A. Pal, S. R. Bhatta and A. Thakur, Recent advances in the development of ferrocene based electroactive small molecules for cation recognition: A comprehensive review of the years 2010–2020, *Coord. Chem. Rev.*, 2021, **431**, 213685.
36 S. Singha, Y. W. Jun, S. Sarkar and K. H. Ahn, An endeavor in the reaction-based approach to fluorescent probes for biorelevant analytes: Challenges and achievements, *Acc. Chem. Res.*, 2019, **52**, 2571–2581.
37 S. Y. Chen, Z. Li, K. Li and X. Q. Yu, Small molecular fluorescent probes for the detection of lead, cadmium and mercury ions, *Coord. Chem. Rev.*, 2021, **429**, 213691.
38 D. Wu, A. C. Sedgwick, T. Gunnlaugsson, E. U. Akkaya, J. Yoon and T. D. James, Fluorescent chemosensors: the past, present and future, *Chem. Soc. Rev.*, 2017, **46**, 7105–7123.
39 K. P. Carter, A. M. Young and A. E. Palmer, Fluorescent sensors for measuring metal ions in living systems, *Chem. Rev.*, 2014, **114**, 4564–4601.
40 Z. Chen, Z. Zhang, J. Qi, J. You, J. Ma and L. Chen, Colorimetric detection of heavy metal ions with various chromogenic materials: Strategies and applications, *J. Hazard. Mater.*, 2023, **441**, 129889.
41 Y. Song, J. Tao, Y. Wang, Z. Cai, X. Fang, S. Wang and H. Xu, A novel dual-responsive fluorescent probe for the detection of copper(II) and nickel(II) based on BODIPY derivatives, *Inorg. Chim. Acta*, 2021, **516**, 120099.
42 A. K. Manna, S. Chowdhury and G. K. Patra, A novel hydrazide-based selective and sensitive optical chemosensor for the detection of Ni^{2+} ions: Applications in live cell imaging, molecular logic gates and smart phone-based analysis, *Dalton Trans.*, 2019, **48**, 12336–12348.
43 M. Sahu, A. K. Manna, S. Chowdhury and G. K. Patra, A novel dihydro phenylquinazolinone-based two-in-one colourimetric chemosensor for nickel(II), copper(II) and its copper complex for the fluorescent colourimetric nanomolar detection of the cyanide anion, *RSC Adv.*, 2020, **10**, 44860–44875.
44 S. Goswami, S. Chakraborty, M. K. Adak, S. Halder, C. K. Quah, H. K. Fun, B. Pakhira and S. Sarkar, A highly selective ratiometric chemosensor for Ni^{2+} in a quinoxaline matrix, *New J. Chem.*, 2014, **38**, 6230–6235.
45 K. Alizadeh, B. Rezaei and E. Khazaeli, A new triazene-1-oxide derivative, immobilized on the triacetyl cellulose membrane as an optical Ni^{2+} sensor, *Sens. Actuators, B*, 2014, **193**, 267–272.
46 G. B. Li, H. C. Fang, Y. P. Cai, Z. Y. Zhou, P. K. Thallapally and J. Tian, Construction of a novel Zn-Ni trinuclear schiff base and a Ni^{2+} chemosensor, *Inorg. Chem.*, 2010, **49**, 7241–7243.
47 F. Otón, M. D. C. González, A. Espinosa, A. Tárraga and P. Molina, Synthesis, structural characterization, and sensing properties of clickable unsymmetrical 1,1′-disubstituted ferrocene-triazole derivatives, *Organometallics*, 2012, **31**, 2085–2096.
48 P. Wang, Z. Li, G. C. Lv, H. P. Zhou, C. Hou, W. Y. Sun and Y. P. Tian, Zinc(II) complex with teirpyridine derivative ligand as 'on-off' type fluorescent probe for cobalt(II) and nickel(II) ions, *Inorg. Chem. Commun.*, 2012, **18**, 87–91.
49 R. Pavadai, A. Amalraj, S. Subramanian and P. Perumal, High catalytic activity of fluorophore-labeled Y-shaped DNAzyme/3D MOF-MoS_2NBs as a versatile biosensing platform for the simultaneous detection of Hg^{2+}, Ni^{2+}, and Ag^{+} ions, *ACS Appl. Mater. Interfaces*, 2021, **13**, 31710–31724.
50 K. Zheng, Z. Q. Liu, Y. Huang, F. Chen, C. H. Zeng, S. Zhong and S. W. Ng, Highly luminescent Ln-MOFs based on 1,3-adamantanediacetic acid as bifunctional sensor, *Sens. Actuators, B*, 2018, **257**, 705–713.
51 B. Qin, X. Zhang and J. Zhang, A new multifunctional zinc-organic framework with rare interpenetrated tripillared bilayers as a luminescent probe for detecting $Ni^{2+}$and PO_4^{3-}in water, *Cryst. Growth Des.*, 2020, **20**, 5120–5128.
52 K. Shrivas, P. Maji and K. Dewangan, Onsite-detection of barium and nickel from river, pond and tap water samples using gold nanoparticles as a chemical sensor, *Spectrochim. Acta, Part A*, 2017, **173**, 630–636.
53 A. Parnsubsakul, S. Oaew and W. Surareungchai, Zwitterionic peptide-capped gold nanoparticles for colorimetric detection of Ni^{2+}, *Nanoscale*, 2018, **10**, 5466–5473.
54 S. J. Yoon, Y. S. Nam, H. J. Lee, Y. Lee and K. B. Lee, Colorimetric probe for Ni^{2+} based on shape transformation of triangular silver nanoprisms upon H_2O_2 etching, *Sens. Actuators, B*, 2019, **300**, 127045.
55 A. Rossi, M. Zannotti, M. Cuccioloni, M. Minicucci, L. Petetta, M. Angeletti and R. Giovannetti, Silver nanoparticle-based sensor for the selective detection of nickel ions, *Nanomaterials*, 2021, **11**, 1–16.
56 D. L. Ma, S. Lin, W. Wang, C. Yang and C. H. Leung, Luminescent chemosensors by using cyclometalated iridium(III) complexes and their applications, *Chem. Sci.*, 2017, **8**, 878–889.
57 K. C. Chang, S. S. Sun, M. O. Odago and A. J. Lees, Anion recognition and sensing by transition-metal complexes with polarized NH recognition motifs, *Coord. Chem. Rev.*, 2015, **284**, 111–123.
58 S. Naithani, F. Thetiot, V. Yadav, S. Saini, P. Roy, S. Layek, T. Goswami and S. Kumar, A pyridyl-benzimidazole based ruthenium(II) complex as optical sensor: Targeted cyanide detection and live cell imaging applications, *J. Photochem. Photobiol., A*, 2024, **453**, 115610.
59 V. W. W. Yam and K. M. C. Wong, Luminescent metal complexes of d^6, d^8 and d^{10} transition metal centres, *Chem. Commun.*, 2011, **47**, 11579–11592.
60 Q. Zhao, H. Huang and F. Li, Phosphorescent heavy-metal complexes for bioimaging, *Chem. Soc. Rev.*, 2011, **40**, 2508–2524.
61 R. L. Mattison, A. A. Bowyer and E. J. New, Small molecule optical sensors for nickel: The quest for a universal nickel receptor, *Coord. Chem. Rev.*, 2020, **425**, 213522.
62 S. Chakraborty and S. Rayalu, Detection of nickel by chemo and fluoro sensing technologies, *Spectrochim. Acta, Part A*, 2021, **245**, 118915.

63 M. Loya, S. Ghosh and A. K. Atta, A review on dual detection of Cu^{2+} and Ni^{2+} ions by using single fluorometric and colorimetric organic molecular probes, *J. Mol. Struct.*, 2023, **1278**, 134949.
64 Y. Zhang, Y. Zhu, Z. Zeng, G. Zeng, R. Xiao, Y. Wang, Y. Hu, L. Tang and C. Feng, Sensors for the environmental pollutant detection: Are we already there?, *Coord. Chem. Rev.*, 2021, **431**, 213681.
65 D. C. Magri, Logical sensing with fluorescent molecular logic gates based on photoinduced electron transfer, *Coord. Chem. Rev.*, 2021, **426**, 213598.
66 Y. L. Pak, Y. Wang and Q. Xu, Conjugated polymer based fluorescent probes for metal ions, *Coord. Chem. Rev.*, 2021, **433**, 213745.
67 Z. Li, J. T. Hou, S. Wang, L. Zhu, X. He and J. Shen, Recent advances of luminescent sensors for iron and copper: Platforms, mechanisms, and bio-applications, *Coord. Chem. Rev.*, 2022, **469**, 214695.
68 G. G. Dias, M. O. Rodrigues, E. R. S. Paz, M. P. Nunes, M. H. Araujo, F. S. Rodembusch and E. N. da Silva Júnior, Aryl-phenanthro[9,10-*d*]imidazole: A versatile scaffold for the design of optical-based sensors, *ACS Sens.*, 2022, **7**, 2865–2919.
69 X. Li, S. S. Rajasree, J. Yu and P. Deria, The role of photoinduced charge transfer for photocatalysis, photoelectrocatalysis and luminescence sensing in metal-organic frameworks, *Dalton Trans.*, 2020, **49**, 12892–12917.
70 L. Wu, C. Huang, B. P. Emery, A. C. Sedgwick, S. D. Bull, X. P. He, H. Tian, J. Yoon, J. L. Sessler and T. D. James, Förster resonance energy transfer (FRET)-based small-molecule sensors and imaging agents, *Chem. Soc. Rev.*, 2020, **49**, 5110–5139.
71 X. Zhang, Y. Hu, X. Yang, Y. Tang, S. Han, A. Kang, H. Deng, Y. Chi, D. Zhu and Y. Lu, Förster resonance energy transfer (FRET)-based biosensors for biological applications, *Biosens. Bioelectron.*, 2019, **138**, 111314.
72 L. Chen, P. Y. Fu, H. P. Wang and M. Pan, Excited-State Intramolecular Proton Transfer (ESIPT) for Optical Sensing in Solid State, *Adv. Opt. Mater.*, 2021, **9**, 1–25.
73 S. Sharma and K. S. Ghosh, Recent advances (2017–20) in the detection of copper ion by using fluorescence sensors working through transfer of photo-induced electron (PET), excited-state intramolecular proton (ESIPT) and Förster resonance energy (FRET), *Spectrochim. Acta, Part A*, 2021, **254**, 119610.
74 X. He, L. H. Xiong, Y. Huang, Z. Zhao, Z. Wang, J. W. Y. Lam, R. T. K. Kwok and B. Z. Tang, AIE-based energy transfer systems for biosensing, imaging, and therapeutics, *TrAC, Trends Anal. Chem.*, 2020, **122**, 115743.
75 P. Alam, N. L. C. Leung, J. Zhang, R. T. K. Kwok, J. W. Y. Lam and B. Z. Tang, AIE-based luminescence probes for metal ion detection, *Coord. Chem. Rev.*, 2021, **429**, 213693.
76 M. Asad, M. I. Anwar, A. Abbas, A. Younas, S. Hussain, R. Gao, L.-K. Li, M. Shahid and S. Khan, AIE based luminescent porous materials as cutting-edge tool for environmental monitoring: State of the art advances and perspectives, *Coord. Chem. Rev.*, 2022, **463**, 214539.
77 A. J. Bryan, A. P. de Silva, S. A. De Silva, R. A. D. D. Rupasinghe and K. R. A. S. Sandanayake, Photo-induced electron transfer as a general design logic for fluorescent molecular sensors for cations, *Biosensors*, 1989, **4**, 169–179.
78 A. P. De Silva, T. S. Moody and G. D. Wright, Fluorescent PET (Photoinduced Electron Transfer) sensors as potent analytical tools, *Analyst*, 2009, **134**, 2385–2393.
79 A. Tarai, Y. Li, B. Liu, D. Zhang, J. Li, W. Yan, J. Zhang, J. Qu and Z. Yang, A review on recognition of tri-/tetra-analyte by using simple organic colorimetric and fluorometric probes, *Coord. Chem. Rev.*, 2021, **445**, 214070.
80 W. Zhang, Z. Ma, L. Du and M. Li, Design strategy for photoinduced electron transfer-based small-molecule fluorescent probes of biomacromolecules, *Analyst*, 2014, **139**, 2641–2649.
81 S. Diao, J. L. Blackburn, G. Hong, A. L. Antaris, J. Chang, J. Z. Wu, B. Zhang, K. Cheng, C. J. Kuo and H. Dai, Fluorescence Imaging In Vivo at Wavelengths beyond 1500 nm, *Angew. Chem.*, 2015, **127**, 14971–14975.
82 S. Diao, G. Hong, A. L. Antaris, J. L. Blackburn, K. Cheng, Z. Cheng and H. Dai, Biological imaging without autofluorescence in the second near-infrared region, *Nano Res.*, 2015, **8**, 3027–3034.
83 Y. Tang, F. Pei, X. Lu, Q. Fan and W. Huang, Recent Advances on Activatable NIR-II Fluorescence Probes for Biomedical Imaging, *Adv. Opt. Mater.*, 2019, **7**, 1–18.
84 L. Wu, J. Liu, P. Li, B. Tang and T. D. James, Two-photon small-molecule fluorescence-based agents for sensing, imaging, and therapy within biological systems, *Chem. Soc. Rev.*, 2021, **50**, 702–734.
85 B. Kaur, N. Kaur and S. Kumar, Colorimetric metal ion sensors – A comprehensive review of the years 2011–2016, *Coord. Chem. Rev.*, 2018, **358**, 13–69.
86 R. G. Pearson, Hard and Soft Acids and Bases, *J. Am. Chem. Soc.*, 1963, **85**, 3533–3539.
87 E. M. Lee, S. Y. Gwon and S. H. Kim, Spectral properties of highly selective chemosensor for Hg^{2+}, *Spectrochim. Acta, Part A*, 2014, **120**, 646–649.
88 R. Rani, K. Paul and V. Luxami, An NBD-based two-in-one Cu^{2+}/Ni^{2+} chemosensor with differential charge transfer processes, *New J. Chem.*, 2016, **40**, 2418–2422.
89 R. D. Shannon, Revised effective ionic radii and systematic studies of interatomic distances in halides and chalcogenides, *Acta Crystallogr., Sect. A: Cryst. Phys., Diffr., Theor. Gen. Crystallogr.*, 1976, **32**, 751–767.
90 T. Chopra, S. Sasan, L. Devi, R. Parkesh and K. K. Kapoor, A comprehensive review on recent advances in copper sensors, *Coord. Chem. Rev.*, 2022, **470**, 214704.
91 F. Wang, K. Wang, Q. Kong, J. Wang, D. Xi, B. Gu, S. Lu, T. Wei and X. Chen, Recent studies focusing on the development of fluorescence probes for zinc ion, *Coord. Chem. Rev.*, 2021, **429**, 213636.

92 S. Kumar, J. Kaushal, T. Goswami, P. Kumar and P. Kumar, Recent progress on synthetic and protein-based genetically encoded sensors for fluorimetric Cu(I) recognition: Binding and reaction-based approaches, *Sens. Diagn.*, 2022, **1**, 429–448.
93 A. Waheed, T. Ahmad, M. Haroon and N. Ullah, A highly sensitive and selective fluorescent sensor for zinc(II) ions based on a 1,2,3-triazolyl-functionalized 2,2′-dipicolylamine (DPA), *ChemistrySelect*, 2020, **5**, 5300–5305.
94 J. E. Kwon, S. Lee, Y. You, K. H. Baek, K. Ohkubo, J. Cho, S. Fukuzumi, I. Shin, S. Y. Park and W. Nam, Fluorescent zinc sensor with minimized proton-induced interferences: Photophysical mechanism for fluorescence turn-on response and detection of endogenous free zinc ions, *Inorg. Chem.*, 2012, **51**, 8760–8774.
95 C. Y. Lin and P. P. Power, Complexes of Ni(I): A 'rare' oxidation state of growing importance, *Chem. Soc. Rev.*, 2017, **46**, 5347–5399.
96 K. Nakajima, K. Nansai, K. Matsubae, M. Tomita, W. Takayanagi and T. Nagasaka, Global land-use change hidden behind nickel consumption, *Sci. Total Environ.*, 2017, **586**, 730–737.
97 E. Denkhaus and K. Salnikow, Nickel essentiality, toxicity, and carcinogenicity, *Crit. Rev. Oncol. Hematol.*, 2002, **42**, 35–56.
98 B. Zambelli and S. Ciurli, Nickel and Human Health, *Interrelations between essential metal ions and human diseases*, ed. A. Sigel, H. Sigel and R. K. O. Sigel, Springer Netherlands, 2013, pp. 321–357.
99 H. Kaluarachchi, K. C. C. Chung and D. B. Zamble, Microbial nickel proteins, *Nat. Prod. Rep.*, 2010, **27**, 681–694.
100 Z. Ma, F. E. Jacobsen and D. P. Giedroc, Coordination chemistry of bacterial metal transport and sensing, *Chem. Rev.*, 2009, **109**, 4644–4681.
101 B. Zambelli, V. N. Uversky and S. Ciurli, Nickel impact on human health: An intrinsic disorder perspective, *Biochim. Biophys. Acta, Proteins Proteomics*, 2016, **1864**, 1714–1731.
102 M. Alfano and C. Cavazza, Structure, function, and biosynthesis of nickel-dependent enzymes, *Protein Sci.*, 2020, **29**, 1071–1089.
103 S. T. Stripp, B. R. Duffus, V. Fourmond, C. Léger, S. Leimkühler, S. Hirota, Y. Hu, A. Jasniewski, H. Ogata and M. W. Ribbe, Second and outer coordination sphere effects in nitrogenase, hydrogenase, formate dehydrogenase, and CO dehydrogenase, *Chem. Rev.*, 2022, **122**, 11900–11973.
104 S. Kumar, S. Singh, A. Kumar and P. Kumar, Recognition, mechanistic investigation and applications for the detection of biorelevant Cu^{2+}/Fe^{2+}/Fe^{3+}ions by ruthenium(II)-polypyridyl based fluorescent sensors, *Dalton Trans.*, 2021, **50**, 2705–2721.
105 G. C. Liu, Y. Li, J. Chi, N. Xu, X. L. Wang, H. Y. Lin and Y. Q. Chen, Multi-functional fluorescent responses of cobalt complexes derived from functionalized amide-bridged ligand, *Dyes Pigm.*, 2020, **174**, 108064.
106 R. Pandey, A. Kumar, Q. Xu and D. S. Pandey, Zinc(II), copper(II) and cadmium(II) complexes as fluorescent chemosensors for cations, *Dalton Trans.*, 2020, **49**, 542–568.
107 P. Tao, S. J. Liu and W. Y. Wong, Phosphorescent manganese(II) complexes and their emerging applications, *Adv. Opt. Mater.*, 2020, **8**, 1–21.
108 G. Q. Jin, Y. Ning, J. X. Geng, Z. F. Jiang, Y. Wang and J. L. Zhang, Joining the journey to near infrared (NIR) imaging: The emerging role of lanthanides in the designing of molecular probes, *Inorg. Chem. Front.*, 2020, **7**, 289–299.
109 J. Liu, G. Ji, J. Xiao and Z. Liu, Ultrastable 1D Europium complex for simultaneous and quantitative sensing of Cr(III) and Cr(VI) ions in aqueous solution with high selectivity and sensitivity, *Inorg. Chem.*, 2017, **56**, 4197–4205.
110 A. M. Lunev and Y. A. Belousov, Luminescent sensor materials based on rare-earth element complexes for detecting cations, anions, and small molecules, *Russ. Chem. Bull.*, 2022, **71**, 825–857.
111 M. L. P. Reddy, V. Divya and K. S. Bejoymohandas, Luminescent lanthanide molecular materials as potential probes for the recognition of toxic and biologically important cations, *Dyes Pigm.*, 2023, **215**, 111248.
112 H. Song, G. Liu, C. Fan and S. Pu, A novel fluorescent sensor for Al^{3+} and Zn^{2+} based on a new europium complex with a 1,10-phenanthroline ligand, *J. Rare Earths*, 2021, **39**, 460–468.
113 A. W. Czarnik, Chemical communication in water using fluorescent chemosensors, *Acc. Chem. Res.*, 1994, **27**, 302–308.
114 Y. Zhang, Y. Zhu, Z. Zeng, G. Zeng, R. Xiao, Y. Wang, Y. Hu, L. Tang and C. Feng, Sensors for the environmental pollutant detection: Are we already there?, *Coord. Chem. Rev.*, 2021, **431**, 213681.
115 A. R. Ii, F. Bolletta, I. Costa, L. Fabbrizzi, M. Licchelli, M. Montalti, P. Pallavicini and N. Zaccheroni, A [RuII(bipy)$_3$]-[1,9-diamino-3,7-diazanonane-4,6-dione] two-component system, as an efficient ON–OFF luminescent chemosensor for Ni^{2+} and Cu^{2+} in water, based on an ET (energy transfer) mechanism, *J. Chem. Soc., Dalton Trans.*, 1999, 1381–1385.
116 S. Ghosh, R. Chakrabarty and P. S. Mukherjee, Design, synthesis, and characterizations of a series of Pt macrocycles and fluorescent sensing of Cu/Ni through metal coordination, *Inorg. Chem.*, 2009, **48**, 3291.
117 M. Bar, S. Deb, A. Paul and S. Baitalik, Stimuli-responsive luminescent bis-tridentate ru(ii) complexes toward the design of functional materials, *Inorg. Chem.*, 2018, **57**, 12010–12024.
118 M. Y. Wen, L. Ren and G. H. Cui, Two Co(ii) complexes containing pyridylbenzimidazole ligands as chemosensors for the sensing of levofloxacin, acetylacetone, and $Ni^{2+}$with high selectivity and sensitivity, *CrystEngComm*, 2021, **23**, 8563–8571.
119 Y. B. Wu, Q. Yu, G. H. Cui and L. Fu, Synthesis, crystal structures, and luminescence sensing properties of two

cobalt(II) complexes containing bis(thiabendazole) moieties, *Transition Met. Chem.*, 2021, **46**, 523–536.

120 L. J. Han, Y. J. Kong, Y. Y. Xu and M. M. Huang, A Zn-based coordination compound for fluorescence detection of Fe^{3+}, Cu^{2+}, Ni^{2+} and CrO_4^{2-} ions, *Polyhedron*, 2021, **193**, 114868.

121 M. J. E. Resendiz, J. C. Noveron, H. Disteldorf, S. Fischer and P. J. Stang, A self-assembled supramolecular optical sensor for Ni(II), Cd(II), and Cr(III), *Org. Lett.*, 2004, **6**, 651–653.

122 P. N. Hishimone, E. Hamukwaya and V. Uahengo, The C 2-symmetry colorimetric dye based on a thiosemicarbazone derivative and its cadmium complex for detecting heavy metal cations (Ni^{2+}, Co^{2+}, Cd^{2+}, and Cu^{2+}) collectively, in DMF, *J. Fluoresc.*, 2021, **31**, 999–1008.

123 N. Stock and S. Biswas, Synthesis of metal-organic frameworks (MOFs): Routes to various MOF topologies, morphologies, and composites, *Chem. Rev.*, 2012, **112**, 933–969.

124 J. Meng, X. Liu, C. Niu, Q. Pang, J. Li, F. Liu, Z. Liu and L. Mai, Advances in metal-organic framework coatings: Versatile synthesis and broad applications, *Chem. Soc. Rev.*, 2020, **49**, 3142–3186.

125 O. K. Farha, I. Eryazici, N. C. Jeong, B. G. Hauser, C. E. Wilmer, A. A. Sarjeant, R. Q. Snurr, S. T. Nguyen, A. Ö. Yazaydin and J. T. Hupp, Metal-organic framework materials with ultrahigh surface areas: Is the sky the limit?, *J. Am. Chem. Soc.*, 2012, **134**, 15016–15021.

126 X. Zhang, Z. Chen, X. Liu, S. L. Hanna, X. Wang, R. Taheri-Ledari, A. Maleki, P. Li and O. K. Farha, A historical overview of the activation and porosity of metal-organic frameworks, *Chem. Soc. Rev.*, 2020, **49**, 7406–7427.

127 H. Kim, C. Rey, M. J. Glimcher, J. B. M. Res, N. L. Rosi, J. Eckert, M. Eddaoudi, T. Vodak, J. Kim, M. O. Keeffe and O. M. Yaghi, Hydrogen storage in microporous metal-organic frameworks, *Science*, 2003, **300**, 1127–1129.

128 Q. Qian, P. A. Asinger, M. J. Lee, G. Han, K. M. Rodriguez, S. Lin, F. M. Benedetti, A. X. Wu, W. S. Chi and Z. P. Smith, MOF-based membranes for gas separations, *Chem. Rev.*, 2020, **120**, 8161–8266.

129 G. M. Espallargas and E. Coronado, Magnetic functionalities in MOFs: From the framework to the pore, *Chem. Soc. Rev.*, 2018, **47**, 533–557.

130 B. E. Meteku, J. Huang, J. Zeng, F. Subhan, F. Feng, Y. Zhang, Z. Qiu, S. Aslam, G. Li and Z. Yan, Magnetic metal–organic framework composites for environmental monitoring and remediation, *Coord. Chem. Rev.*, 2020, **413**, 213261.

131 E. Linnane, S. Haddad, F. Melle, Z. Mei and D. Fairen-Jimenez, The uptake of metal-organic frameworks: a journey into the cell, *Chem. Soc. Rev.*, 2022, **51**, 6065–6086.

132 Y. Chen, P. Li, J. A. Modica, R. J. Drout and O. K. Farha, Acid-resistant mesoporous metal-organic framework toward oral insulin delivery: Protein encapsulation, protection, and release, *J. Am. Chem. Soc.*, 2018, **140**, 5678–5681.

133 M. Ding, R. W. Flaig, H. L. Jiang and O. M. Yaghi, Carbon capture and conversion using metal-organic frameworks and MOF-based materials, *Chem. Soc. Rev.*, 2019, **48**, 2783–2828.

134 X. Zhang, Z. Huang, M. Ferrandon, D. Yang, L. Robison, P. Li, T. C. Wang, M. Delferro and O. K. Farha, Catalytic chemoselective functionalization of methane in a metal-organic framework, *Nat. Catal.*, 2018, **1**, 356–362.

135 V. Stavila, A. A. Talin and M. D. Allendorf, MOF-based electronic and opto-electronic devices, *Chem. Soc. Rev.*, 2014, **43**, 5994–6010.

136 X. Ren, G. Liao, Z. Li, H. Qiao, Y. Zhang, X. Yu, B. Wang, H. Tan, L. Shi, X. Qi and H. Zhang, Two-dimensional MOF and COF nanosheets for next-generation optoelectronic applications, *Coord. Chem. Rev.*, 2021, **435**, 213781.

137 S. A. A. Razavi and A. Morsali, Metal ion detection using luminescent-MOFs: Principles, strategies and roadmap, *Coord. Chem. Rev.*, 2020, **415**, 213299.

138 L. E. Kreno, K. Leong, O. K. Farha, M. Allendorf, R. P. Van Duyne and J. T. Hupp, Metal-organic framework materials as chemical sensors, *Chem. Rev.*, 2012, **112**, 1105–1125.

139 S. Kamal, M. Khalid, M. S. Khan and M. Shahid, Metal organic frameworks and their composites as effective tools for sensing environmental hazards: An up to date tale of mechanism, current trends and future prospects, *Coord. Chem. Rev.*, 2023, **474**, 214859.

140 H. N. Wang, S. Q. Jiang, Q. Y. Lu, Z. Y. Zhou, S. P. Zhuo, G. G. Shan and Z. M. Su, A pillar-layer MOF for detection of small molecule acetone and metal ions in dilute solution, *RSC Adv.*, 2015, **5**, 48881–48884.

141 Y. Xia, K. L. Cao, M. M. Han and Y. L. Feng, Highly selective CH_2Cl_2 fluorescent sensor based on Cd(II) metal-organic framework, *Inorg. Chem. Commun.*, 2015, **56**, 76–78.

142 M. L. Aulsebrook, B. Graham, M. R. Grace and K. L. Tuck, Lanthanide complexes for luminescence-based sensing of low molecular weight analytes, *Coord. Chem. Rev.*, 2018, **375**, 191–220.

143 S. Naithani, T. Goswami, F. Thetiot and S. Kumar, Imidazo[4,5-*f*,][1,10]phenanthroline based luminescent probes for anion recognition: Recent achievements and challenges, *Coord. Chem. Rev.*, 2023, **475**, 214894.

144 S. E. Bodman and S. J. Butler, Advances in anion binding and sensing using luminescent lanthanide complexes, *Chem. Sci.*, 2021, **12**, 2716–2734.

145 M. D. Ward, Mechanisms of sensitization of lanthanide (III)-based luminescence in transition metal/lanthanide and anthracene/lanthanide dyads, *Coord. Chem. Rev.*, 2010, **254**, 2634–2642.

146 F. F. Chen, Z. Q. Chen, Z. Q. Bian and C. H. Huang, Sensitized luminescence from lanthanides in d-f bimetallic complexes, *Coord. Chem. Rev.*, 2010, **254**, 991–1010.

147 M. D. Ward, Transition-metal sensitised near-infrared luminescence from lanthanides in d-f heteronuclear arrays, *Coord. Chem. Rev.*, 2007, **251**, 1663–1677.

148 Y. Wang, X. G. Wang, B. Yuan, C. Y. Shao, Y. Y. Chen, B. B. Zhou, M. S. Li, X. M. An, P. Cheng and X. J. Zhao, Cation-exchange porosity tuning in a dynamic 4d-4f-3d framework for NiII ion-selective luminescent probe, *Inorg. Chem.*, 2015, **54**, 4456–4465.

149 J. J. Li, T. T. Fan, X. L. Qu, H. L. Han and X. Li, Temperature-induced 1D lanthanide polymeric frameworks based on Lnn (n = 2, 2, 4, 6) cores: Synthesis, crystal structures and luminescence properties, *Dalton Trans.*, 2016, **45**, 2924–2935.

150 Z. Chen, X. Xing, R. Zhou, D. Wang, X. Ye, B. Li and D. Wu, Highly selective detection of Ni^{2+} ion based on a luminescent Zn(II) coordination polymer, *IEEE Sens. J.*, 2019, **19**, 7652–7658.

151 H. N. Rubin and M. M. Reynolds, Amino-incorporated Tricarboxylate metal-organic framework for the sensitive fluorescence detection of heavy metal ions with insights into the origin of photoluminescence response, *Inorg. Chem.*, 2019, **58**, 10671–10679.

152 J. Peng, W. Zhou, H. Ding, H. Du and S. J. Li, Surface-effect on detection ability of fluorescent Eu(btc) metal-organic frameworks to metal ions, *J. Rare Earths*, 2021, **39**, 446–452.

153 L. Guan, Z. Jiang, Y. Cui, Y. Yang, D. Yang and G. Qian, An MOF-based luminescent sensor array for pattern recognition and quantification of metal ions, *Adv. Opt. Mater.*, 2021, **9**, 1–7.

154 B. Kabak and E. Kendüzler, Europium metal-organic frameworks: Synthesis, characterization, and application as fluorescence sensors for the detection of Cu^{2+}, Ni^{2+} cations and T3, T4 hormones, *Talanta*, 2024, **266**, 124944.

155 D. Mei and B. Yan, Flumequine-mediated fluorescent zeolitic imidazolate framework functionalized by Eu^{3+} for sensitive and selective detection of UO_2^{2+}, Ni^{2+} and Cu^{2+} in nuclear wastewater, *J. Hazard. Mater.*, 2023, **447**, 130822.

156 J. Xu, T. Liu, X. Han, S. Wang, D. Liu and C. Wang, Construction of a porous three dimensional rare earth metal-sulfur-ligand open framework, *Chem. Commun.*, 2015, **51**, 15819–15822.

157 L. Ding, L. H. Liu, Q. Shi, Y. Q. Sun, Y. J. Wang and Y. P. Chen, Luminescent 3D lanthanide-cadmium heterometal-organic frameworks with chemical stability and selective luminescent sensing, *Inorg. Chem.*, 2017, **56**, 14850–14858.

158 Z. Zhang, Y. Lou, C. Guo, Q. Jia, Y. Song, J. Y. Tian, S. Zhang, M. Wang, L. He and M. Du, Metal–organic frameworks (MOFs) based chemosensors/biosensors for analysis of food contaminants, *Trends Food Sci. Technol.*, 2021, **118**, 569–588.

159 L. Huang, R. Shen and Q. Shuai, Adsorptive removal of pharmaceuticals from water using metal-organic frameworks: A review, *J. Environ. Manage.*, 2021, **277**, 111389.

160 H. He, Q. Q. Zhu, C. P. Li and M. Du, Design of a highly-stable pillar-layer zinc(II) porous framework for rapid, reversible, and multi-responsive luminescent sensor in water, *Cryst. Growth Des.*, 2018, **19**, 694–703.

161 Y. Yu, G. Li, J. Liu and D. Yuan, A recyclable fluorescent covalent organic framework for exclusive detection and removal of mercury(II), *Chem. Eng. J.*, 2020, **401**, 126139.

